frontiers | Frontiers in Earth Science

TYPE Methods
PUBLISHED 07 October 2024
DOI 10.3389/feart.2024.1438382

OPEN ACCESS

EDITED BY
Carmen Sanchez-Valle,
University of Münster, Germany

REVIEWED BY
Stéphane Affolter,
University of Basel, Switzerland
Tobias Fusswinkel,
RWTH Aachen University, Germany

*CORRESPONDENCE
Orlando Sébastien Olivieri,
orlando.olivieri2@unibo.it

RECEIVED 25 May 2024
ACCEPTED 18 September 2024
PUBLISHED 07 October 2024

CITATION
Olivieri OS, Marassi V, Casolari S, Sissman O, Daniel I, Fiebig J and Vitale Brovarone A (2024) Protocols for bulk off-line fluid inclusion extraction for the analysis of δ^{13}C-CH_4 and δ^{13}C-CO_2 using a cavity ring-down spectroscopy (CRDS) analyser. *Front. Earth Sci.* 12:1438382. doi: 10.3389/feart.2024.1438382

Protocols for bulk off-line fluid inclusion extraction for the analysis of δ^{13}C-CH_4 and δ^{13}C-CO_2 using a cavity ring-down spectroscopy (CRDS) analyser

Orlando Sébastien Olivieri[1]*, Valentina Marassi[2], Sonia Casolari[2], Olivier Sissman[3], Isabelle Daniel[4], Jens Fiebig[5] and Alberto Vitale Brovarone[1,6,7]

[1]Department of Biological, Geological, and Environmental Sciences, Università degli Studi di Bologna, Bologna, Italy, [2]Department of Chemistry "Giacomo Ciamician", Università degli Studi di Bologna, Bologna, Italy, [3]IFP Energies nuovelles, Reuil Malmaison, France, [4]Université Claude Bernard Lyon1, LGL-TPE, UMR 5276, Centre national de la recherche scientifique, Ens de Lyon, Université Jean Monnet Saint-Etienne, Villeurbanne, France, [5]Institut für Geowissenschaften, Goethe-Universität Frankfurt, Frankfurt am Main, Germany, [6]Sorbonne Université, Muséum National d'Histoire Naturelle, UMR CNRS 7590, IRD, Institut de Minéralogie, de Physique des Matériaux et de Cosmochimie, IMPMC, Paris, France, [7]Istituto di Geoscienze e Georisorse, Consiglio Nazionale delle Ricerche, Pisa, Italy

Fluid inclusions are a window into deep geological fluids, providing unique access to their nature and composition. The isotopic composition of CO_2 and CH_4 hosted in fluid inclusions is a powerful proxy to assess the origin and transformation of deep geological fluids, giving insights into carbon sources, fluxes, and degassing in a wide variety of geodynamic settings. Over the last 5 decades, techniques have been developed to extract fluid inclusions from their host minerals and measure their bulk composition. These techniques are often challenged by analytical artifacts including high blank levels of CO_2 and CH_4, fluid re-speciation, gas adsorption, and diffusion. Since these processes may alter the pristine composition of gases liberated from fluid inclusions, rigorous protocols are needed in order to evaluate the isotopic integrity of the extracted volatile species. In this study, we introduce new protocols for bulk off-line fluid inclusion extraction for the analysis of δ^{13}C-CH_4 and δ^{13}C-CO_2 using a Cavity Ring-Down Spectroscopy (CRDS) analyser (Picarro G2201-i). Two mechanical fluid extraction techniques are compared: ball milling in ZrO_2 jars and sample crushing in a stainless steel sealed tube under a hydraulic press. Blanks and isotopically labelled tests with the ball milling technique suggest that rotation speed, grinding stock filling degree and filling type alter the CH_4 and CO_2 concentrations and isotopic compositions measured by the CRDS analyser. In contrast, the crushing technique does not generate measurable quantities of blank CH_4 and CO_2. The protocols presented in this study allow to extract, detect, and analyse δ^{13}C of CH_4 and CO_2 for concentrations above 10 and 1,000 ppm respectively. Interlaboratory experiments allowed to replicate previously measured δ^{13}C-CH_4 values in natural fluid inclusions within 1‰ with both extraction techniques. This study highlights the potential of combining simple bulk off-line fluid inclusion extraction techniques with

a CRDS analyser for $\delta^{13}C$ analysis of CO_2 and CH_4 without gas separation being required.

KEYWORDS

carbon isotope analysis of fluid inclusions, fluid inclusion mechanical extraction, isotopic labelling and interlaboratory comparison, CRDS, natural CH_4 and CO_2

1 Introduction

The analysis and interpretation of geologic degassing of deep volatiles combines information from various disciplines, from the final products of degassing at the Earth's surface, to their source regions in the deep Earth (Andersen and Neumann, 2001; Becker et al., 2008; Bräuer et al., 2016; Crossey et al., 2009; Kerrick and Caldeira, 1998; Lee et al., 2019; Nadeau et al., 1993; Sobolev et al., 2019). The production and migration of deep fluids can be assessed from the study of rock-forming minerals or melts, or from the analysis of fluid inclusions trapped in rocks and minerals from various depths inside the Earth. Fluid inclusions are small cavities inside minerals, usually micrometric in size, filled with paleo-geological fluids (Roedder, 1984; Touret and Frezzotti, 2003; van den Kerkhof et al., 2014). They provide unique access to the nature and composition of deep geological fluids. Fluid inclusions have been described in rocks formed in a wide variety of geodynamic settings: sedimentary environments, low to high grade metamorphic settings, upper mantle conditions, ore deposits, intrusive and extrusive rocks, and extra-terrestrial environments (Andersen and Neumann, 2001; Audétat et al., 1998; Goldstein, 2001; Hansteen and Schmincke, 1998; Roedder, 1984; Scambelluri and Philippot, 2001; Touret and Dietvorst, 1983; Touret and Frezzotti, 2003; van den Kerkhof et al., 2014; Zolensky et al., 2017).

Fluid inclusions may host a large variety of compounds such as H_2O, CO_2, CH_4, N_2, H_2, H_2S, SO_2, COS, CO, O_2, and NH_3 (Frezzotti et al., 2012; Roedder, 1984). Among them, CO_2 and CH_4 are the most common carbon-bearing compounds (Frezzotti et al., 2012). The study of these molecules is critical due to their primary role in the carbon cycle and their impact on Earth's evolution and habitability (Calvin et al., 2023; Fullerton et al., 2019; Hazen and Schiffries, 2013).

The isotopic composition of CO_2 and CH_4 hosted in fluid inclusions is a powerful proxy to assess the origin and evolution of paleo-geological fluids (Beeskow et al., 2006; Etiope et al., 2018; Graser et al., 2008; Grozeva et al., 2020; Luciani et al., 2022; Lüders et al., 2012; Mangenot et al., 2021; Potter and Longstaffe, 2007; Shi et al., 2005). The study of fluid inclusions gives the unique opportunity to assess individual fluid pulses in hydrothermal systems in a wide range of crustal (Audétat et al., 1998; Touret and Dietvorst, 1983) and upper mantle conditions (Andersen and Neumann, 2001; Frezzotti and Touret, 2014; Hansteen and Schmincke, 1998).

Fluid inclusions rich in CO_2 have been documented in a wide variety of contexts, spanning mantle to magmatic, metamorphic, and sedimentary settings (Andersen and Neumann, 2001; Guilhaumou et al., 1984; Hollister, 1988; Lamb et al., 1987; Luciani et al., 2022; Lüders et al., 2012; Smith et al., 2015). Conversely, reduced molecules such as CH_4, higher hydrocarbons, H_2S, H_2 and NH_3 are documented in fluid inclusions hosted in sedimentary (Goldstein, 2001; Mangenot et al., 2021; Tarantola et al., 2007; Wang et al., 2022), as well as crystalline rock including ultramafic (Andreani et al., 2023; Arai et al., 2012; Boutier et al., 2024; Boutier et al., 2021; Grozeva et al., 2020; Klein et al., 2019; Peretti et al., 1992; Vitale Brovarone et al., 2020; Vitale Brovarone et al., 2017; Zhang et al., 2022; Zhang et al., 2021), mafic (Ferrando et al., 2010; Grozeva et al., 2020; Kelley and Früh-Green, 2001; Klein et al., 2019; Normand and Williams-Jones, 2007) and peralkaline igneous rocks (Gottikh et al., 2006; Graser et al., 2008; Nivin, 2019; Potter et al., 2004).

Since different generations of fluid inclusions, representative of different fluid pulses, might be present in the same sample (Roedder, 1984; Touret and Frezzotti, 2003; van den Kerkhof et al., 2014; Zhang et al., 2021), the analysis of volatiles hosted in single fluid inclusions should be preferred over bulk measurements that integrate over several generations of fluid inclusions. Recent advances have been made towards the *in situ* measurement of $\delta^{13}C$ of CO_2 hosted in single fluid inclusions through Raman spectroscopy (Arakawa et al., 2007; Cui et al., 2021; Remigi et al., 2023; Wang and Lu, 2023). Nevertheless, currently, there are no established protocols to measure $\delta^{13}C$-CH_4 of single fluid inclusions through this technique. Alternatively, laser ablation (LA) coupled with gas chromatography-mass spectrometry (GC-MS) has been used to extract and identify alkanes and aromatic hydrocarbons hosted in single petroleum fluid inclusions (Volk et al., 2010). Despite the potential of LA for *in situ* fluid inclusion extraction, Lambrecht et al. (2008) reported laser-induced modification of gas speciation in fluid inclusions that occurred in close proximity to the ablation pits. These authors related the appearance of O_2, H_2 and CO in neighbouring inclusions to the photo-dissociation of H_2O and CO_2. Such laser-induced reactions could affect the isotopic composition of CO_2 and CH_4 hosted in fluid inclusions leading to analytical artifacts.

Based on these limitations, bulk fluid inclusion extraction remains the most frequently used approach to extract gases hosted in fluid inclusions and to measure their isotopic composition. Extraction of bulk fluid inclusion compounds is achieved in two ways, through thermal decrepitation and mechanical extraction. Thermal decrepitation involves heating the sample to high temperatures (usually up to 1,000°C) under vacuum to release all volatile constituents from the inclusions (Abell et al., 1970; Mullis et al., 1994; Norman and Sawkins, 1987; Petersilie and Sörensen, 1970; Piperov and Penchev, 1973), while mechanical extraction consists of the release of fluid inclusion by crushing or milling the sample *in vacuo* or in inert gases (Andrawes and Gibson, 1979; Etiope et al., 2018; Grozeva et al., 2020; Kita, 1981; Norman and Sawkins, 1987; Petersilie and Sörensen, 1970; Piperov and Penchev, 1973; Sanz-Robinson et al., 2021; Stuart and Turner, 1992; Welhan, 1988).

Besides the mixing of multiple fluid inclusion populations (Blamey, 2012; Villa, 2001), the main challenges of fluid inclusion

extraction techniques concern the production of blank gas species (Andrawes and Gibson, 1979; Etiope et al., 2018; Grozeva et al., 2020; Norman and Sawkins, 1987; Piperov and Penchev, 1973; Welhan, 1988), chemical re-equilibration (Piperov and Penchev, 1973), incomplete extraction due to partial adsorption (Barker and Torkelson, 1975; Norman and Sawkins, 1987; Welhan, 1988) and diffusion (Zhang et al., 2014). All of these processes can potentially alter the composition of gases extracted from fluid inclusions. Nevertheless, to our knowledge, very few works have yet reported isotopic labelling experiments (Sanz-Robinson et al., 2021) or interlaboratory comparisons (Etiope et al., 2018; Luciani et al., 2022; Potter and Longstaffe, 2007) to evaluate the preservation of CO_2 and CH_4 carbon isotopic composition after the extraction. Therefore, isotopic labelling experiments and interlaboratory comparisons are necessary steps in the development of rigorous fluid inclusion extraction protocols.

Recently, several protocols have been developed to combine fluid inclusion extraction techniques with CRDS for the isotope analysis of H_2O hosted in fluid inclusions (Affolter et al., 2014; Arienzo et al., 2013; de Graaf et al., 2020; Weissbach et al., 2023). The CRDS system is low-cost compared to GC-IRMS and it guarantees high accuracy and fast measurements. Despite the availability of CRDS systems for $\delta^{13}C$ measurement of CO_2 and CH_4, only two studies (Boutier et al., 2024; Etiope et al., 2018) applied this analytical technique to characterize carbon stable isotope composition of natural fluid inclusions.

In this work we try to fill these gaps by presenting a protocol for bulk off-line fluid inclusion extraction for the analysis of $\delta^{13}C$-CO_2 and $\delta^{13}C$-CH_4 using a Cavity Ring-Down Spectroscopy (CRDS) analyser (Picarro G2201-i). Two mechanical fluid extraction techniques were compared: ball milling in ZrO_2 jars, and sample crushing in a stainless steel sealed tube under a hydraulic press. We tested the different protocols through blanks, isotopic labelling of CH_4 and CO_2, interlaboratory and inter-technique comparisons.

2 Materials and methods

2.1 Extraction apparatus

The ball milling extraction apparatus consists of two 250 mL zirconium oxide (ZrO_2) Retsch™ jars equipped with three ZrO_2 Retsch™ balls (Ø: 30 mm) and an aeration lid (Figures 1A–D). This material was chosen in order minimize the carbon content of the extraction apparatus, that can reach up to 1.2 wt% in stainless steel (upper concentration limit for stainless steel in the European Standard EN 10020–2000 for grades of steel definition and classification). The aeration lid was modified to couple two Swagelok® Quick-Connect stems allowing fast and easy connection with the gas and vacuum lines. To keep the jar sealed during extractions, the nuts and fittings connected to the jar lid were coupled with FMK O-rings guaranteeing good temperature resistance (up to 200°C). The ball milling was carried out with a Retsch™ PM-400 planetary mill. Gas samples were extracted from the jar with gas chromatography syringes with volumes ranging between 250 µL and 25 mL piercing through a rubber septum coupled with a Swagelok® UltraTorr fitting connected to the jar (Figure 1D). Additionally, gas samples were extracted from the jar by expansion of the gas to pre-evacuated Pyrex® bottles connected to the jar through a Swagelok® UltraTorr fitting.

The second apparatus consists of a 35 cm-long stainless steel tube (grade SS-316), (inner diameter ID: 9 mm; outer diameter OD: 12.7 mm) sealed with a stainless steel cap at one end of the tube (Figure 2). The other end is connected to a ball valve and a rubber septum for syringe gas extraction. Further details regarding the components of the extraction apparatus are provided in Supplementary Figure S1; Supplementary Table S1.

2.2 Gases

The mechanical extraction was performed under an atmosphere of Zero Air, consisting in a O_2-N_2 mixture, and under a He atmosphere, both purchased from SIAD™ s.p.a. (Figure 1B). The isotopic labelling experiments were performed using two secondary standards purchased from SIAD™ s.p.a. with the following compositions: CH_4: 10.7 ppmv - CO_2: 504 ppmv - O_2: 20.91 vol% - N_2: Remaining - $\delta^{13}C$-CH_4: 44.6‰+/-0.3‰ - $\delta^{13}C$-CO_2: 8.7‰+/-0.3‰; CH_4: 52.1 ppmv - CO_2: 1,005 ppmv - O_2: 20.84 vol% - N_2: Remaining - $\delta^{13}C$-CH_4: 44.6‰+/-0.3‰ - $\delta^{13}C$-CO_2: 8.7‰+/−0.3‰. The instrumental calibration of the isotopic analyser was achieved through two to three replicated measurements of the abovementioned secondary standards and the following CH_4 and CO_2 isotopic primary standards furnished by Airgas inc.: CH_4: 1,000 ppm - $\delta^{13}C$-CH_4: 68.6+/−0.3‰ - Remaining: zero air; CH_4: 1,000 ppm - $\delta^{13}C$-CH_4: 0.3‰+/-0.3‰ - Remaining: zero air; CO_2: 3 vol% - $\delta^{13}C$-CO_2: 19.7+/−0.5‰ - Remaining: zero air; CO_2: 3 vol% - $\delta^{13}C$-CO_2: +21.0+/−0.5‰ - Remaining: zero air.

2.3 Qualitative and quantitative measurements of gas concentrations and $\delta^{13}C$ compositions

The CO_2 and CH_4 concentrations, expressed in ppm and $\delta^{13}C$-CH_4 and $\delta^{13}C$-CO_2 isotopic composition, expressed in ‰ relative to Vienna PDB (VPDB), of the gas samples were measured with a Cavity Ring-Down Spectrometer (CRDS) Picarro™ G2201-i at the Deep Carbon Lab (University of Bologna). This isotopic analyser allows simultaneous measurement of CO_2 and CH_4 with an accuracy of 200 ppb for CO_2 and 5 ppb for CH_4, < 0.06‰ for $\delta^{13}C$-CH_4 at 10 ppm, and < 0.16‰ for $\delta^{13}C$-CO_2 at 380 ppm. The Picarro™ G2201-i spectrometer allows the measurement of $\delta^{13}C$-CH_4 for samples with low CH_4 concentrations (1.2–15 ppm) in the High Precision mode (HP) and high concentrations (1.2–1,500 ppm) in the High Range mode (HR). The samples were introduced in the analyser through the Picarro™ A0314 Small Sample Introduction Module 2 (SSIM2) which has an internal volume of 20 mL allowing controlled sample dilution in a Zero Air matrix (O_2-N_2) for small sample volumes (Figure 1E). The SSIM2 module specifications guarantee a precision of < 1 ppm for CO_2 (at 400 ppm) and < 3 ppb for CH_4 (at 2 ppm), and $\delta^{13}C$-CH_4 < 0.3‰ at 10 ppm; $\delta^{13}C$-CO_2 < 0.5‰ at 500 ppm.

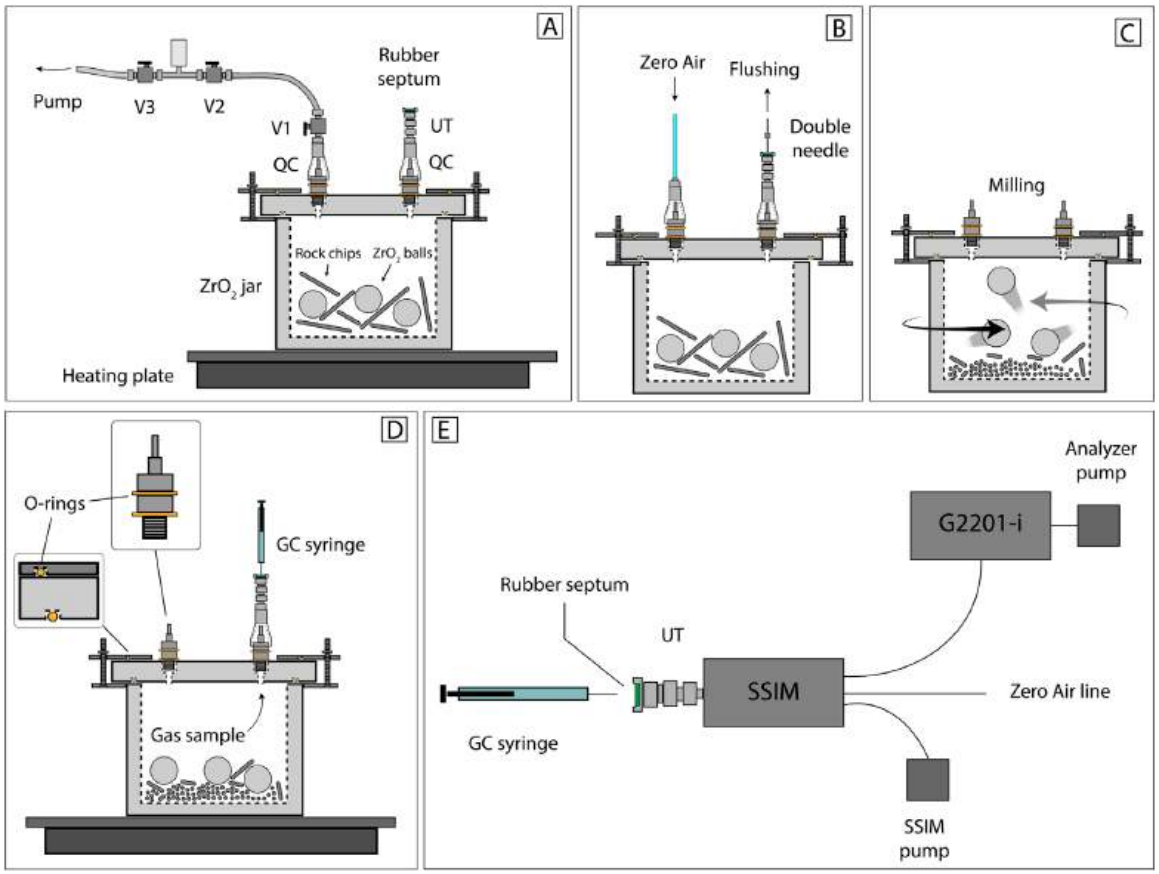

FIGURE 1
The ball milling extraction apparatus. Panels **(A)**, **(B)**, **(C)**, and **(D)** show the steps of the mechanical extraction protocol: **(A)** jar evacuation; **(B)** jar flushing and pumping with Zero Air; **(C)** milling; **(D)** sample extraction after milling; **(E)** sample injection in the SSIM2 Module connected to a G2201-I Picarro analyser. The FMK O-rings present in the extraction apparatus are coloured in yellow (detail in panel (D)). Abbreviations: V1, V2, V3: valves; QC: Swagelok Quick Connect fitting; UT: Ultra Torr.

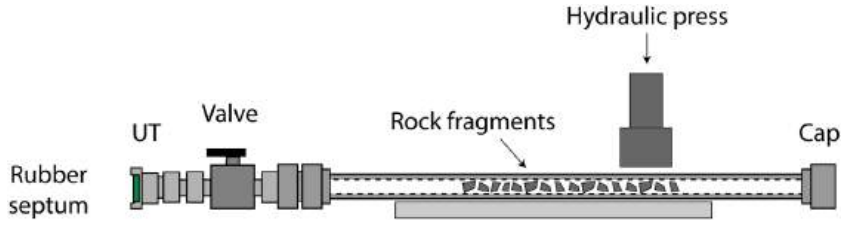

FIGURE 2
The crushing extraction apparatus. The stainless steel tube hosts the sample, it is closed with a cap on one extremity and with a ¼" ball valve on the other extremity. Crushing is operated through a hydraulic press. The gas sample is extracted through an Ultra Torr coupled with a rubber septum (green). Abbreviations: UT: Ultra Torr.

We conducted inter-technique comparison tests by performing bulk δ^{13}C-CH_4 measurements on three gas samples through Gas-Chromatography Mass Spectrometry (GC-IRMS) with a MAT 253 at the Goethe University (Frankfurt am Main). The mass spectrometer was calibrated through the measurement of three isotopic standards furnished by Arndt Schimmelmann (Indiana University). The analyses were performed both through direct expansion of the sample into a loop connected to the GC, or through cryogenic separation of CH_4 using the protocol described by Fiebig et al. (2015). The duplicate analyses were performed by ball milling of a different subset of sample under a He atmosphere (see Section 2.2) at the Deep Carbon Lab (Bologna University).

The composition of blanks (as defined in section 2.6) was also analysed using gas chromatography-thermal conductivity detector (GC-TCD). The analyses were conducted at the

laboratory of analytical chemistry of the "Giacomo Ciamician" chemistry Department in Ravenna with an in-house method available in the laboratory that exploited three in-series columns: HAYESEP N 80–100 MESH, HAYESEP Q 80–100 MESH, Mol. Sieve 5A 60–80 (Veen et al., 2020). The injection volume was set as 250 µL. Peak attribution was achieved via injection of standard gas O_2, N_2, CO_2 and CH_4.

2.4 Petrographic analysis

Petrographic analysis of fluid inclusions was performed at the Deep Carbon Lab (University of Bologna), with a Zeiss AxioScope5 and a Zeiss AxioScope7 petrographic microscopes equipped with Neofluar 50x and 100x objectives.

2.5 Raman spectroscopy

Raman spectroscopy characterization of the fluid inclusions was carried out at the BiGeA department (University of Bologna) using a WITec Alpha 300-R confocal micro-Raman spectrometer with a 532 nm laser source. The Raman shift was calibrated with a Hg-Ar lamp. Raman spectra were acquired with the following parameters: 600 g/mm grating; 20–35 mW laser power on the sample; acquisition duration between 1 and 5 min.

2.6 Synthetic and natural materials for the tests

The material selected for blanks include: 6 mm-thick industrial glass and 6 mm-thick slices of Novate granite, that is a peraluminous leucocratic two-mica granite from the Central Alps (Liati et al., 2000). Industrial glass was selected for blank experiments as a fluid inclusion-free synthetic material. The Novate granite was selected since optical microscopy and Raman spectroscopy characterization in thin section at the BiGeA Department at the Bologna University (Italy) revealed the presence of rare 5–20 µm large biphasic (liquid + vapor) plagioclase-hosted fluid inclusions (Supplementary Figure S2) hosting H_2O and minor amounts of N_2. Neither CO_2 nor CH_4 was detected (Supplementary Figure S3).

Two tests with natural samples hosting CH_4-rich fluid inclusions were chosen for interlaboratory comparison. The first test was carried out on samples of quartz crystals from Val d'Illiez (Swiss Alps), which had been previously characterized by Mangenot et al. (2021). These authors identified both liquid and vapor-rich fluid inclusions hosting H_2O + CH_4 +/− CO_2 based on Raman spectroscopy (Mangenot et al., 2021) (Figure 3A). The authors extracted the volatiles by mechanical crushing under vacuum inside an electromagnet device and measured the δ^2H, $\delta^{13}C$, $^{12}CH_2D_2$ and $^{13}CH_3D$ of methane with a Thermo™ Ultra MAT253 IRMS (Mangenot et al., 2021). The $\delta^{13}C$-CH_4 showed good homogeneity among six samples (avg: 28.5‰; 1σ = 0.4‰).

The second test was performed on a sample of partially serpentinized peridotite (V18-2A) from the Belvidere Mountain Complex (Vermont) that was previously characterized by Boutier et al. (2024); Boutier et al. (2021). The peridotite sample bears gaseous fluid inclusions hosted in olivine (Figure 3B), containing CH_4 and minor amounts of N_2 and NH_3 (Boutier et al., 2024; Boutier et al., 2021) identified by Raman spectroscopy. The authors extracted the volatiles mechanically by ball milling (rotation speed: 700 rpm–duration: 8 min) under a N_2 atmosphere inside a Fritsch 125 mL ZrO_2 jar. The gases were analyzed with a CRDS analyser (Picarro G-2210-i) for $\delta^{13}C$-CH_4 and C_1/C_2. A replication of the analysis was performed with GC-IRMS for $\delta^{13}C$-CH_4 and δ^2H-CH_4 measurement. Both analytical techniques produced indistinguishable results with $\delta^{13}C$-CH_4 values of −12.66+/-0.07‰ and −12.93+/-0.6‰ for CRDS and GC-IRMS, respectively.

Additional samples of variably serpentinized peridotites, and serpentinites crosscut by carbonate veins coming from the Belvidere Mountain Complex (Vermont) were selected for inter-technique comparisons (Supplementary Section S4 for geological context). These samples were chosen either because they contained similar generations of fluid inclusions or due to the rarity of CH_4-rich fluid inclusions, as determined through optical microscopy and Raman spectroscopy analysis of thin sections (Supplementary Figures S4, S5, S6, S7, S8).

2.7 Sample preparation

The rock samples used for fluid inclusion extraction were cut into 6 mm thick slices and weathered surfaces were removed to avoid contamination in the jar. The use of thin slices of rock provided material that could be efficiently crushed to release fluid inclusions. Prior to milling, the rock slices were washed in ultrasonicated bath of distilled water for 10 min at 30°C and dried in an oven at 70°C for 12 h. During sample preparation we purposely avoided the use of any organic solvents which can affect measurements of low-boiling gas species such as CO_2 (Mironova, 2010).

2.8 Protocol description

Between 50 and 113 g of filling materials loaded in the jar, corresponding to approximately 7% and 15% of the jar volume, respectively. The jar was connected to a turbomolecular pump and placed on a heating plate at 70°C to facilitate gas desorption on rock and jar surfaces and to remove atmospheric gases. The evacuation of the jar proceeded until an internal pressure in the range of 1–200 Pa was reached (Figure 1A). The jar was then connected to a flow of Zero Air (O_2-N_2 mix) for CRDS or He for GC-IRMS analysis, flushed for 1 min and pumped at a gauge pressure of 110 kPa (Figure 1B), corresponding to an internal absolute pressure of 210 kPa. A slight overpressure inside the jar during the extraction was adopted rather than vacuum to avoid inflow of ambient air during the experiment. This choice implies the dilution of the extracted gas in the gas matrix. The concentration of CO_2 and CH_4 in the extraction apparatus was monitored before every experiment by extracting 20 mL of gas and ranged between CH_4: 0.01–0.07 ppm and CO_2: 7–15 ppm (Supplementary Table S1). The milling was conducted at variable rotation speeds of 50–400 rpm (maximum speed of the planetary mill used in this study) with breaks and inversion in rotation direction every 30 s. A milling duration of

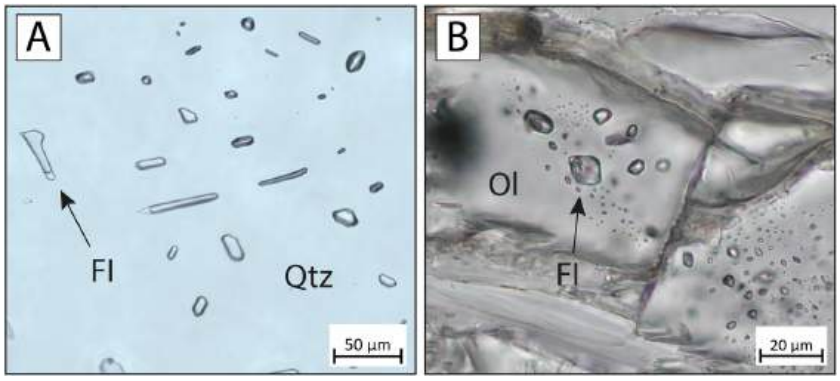

FIGURE 3
Photomicrographs of representative fluid inclusions hosted in the samples analysed in the interlaboratory comparison experiment. Panel **(A)** shows a cluster of monophasic (vapor) and biphasic (liquid + vapor) fluid inclusions hosted in a Val d'Illiez quartz crystal. Panel **(B)** shows trails of monophasic (vapor) olivine-hosted fluid inclusions in sample V18-2A. Abbreviations: Fl = fluid inclusion; Ol = olivine; Qtz = quartz.

3 min was used in all the experiments, longer milling duration was avoided in order to minimize frictional heating (Figure 1C). The details of the milling parameters of every experiment are given in section 3. After the milling, the jar was placed again on a heating plate at 70°C to facilitate the desorption of extracted gases from the newly formed surfaces (Figure 1D). The gas samples were extracted from the jars for the analysis 5–10 min after the end of the milling. After each milling experiment the jar surfaces and the balls were cleaned by milling Fontainebleau quartz sand at 400 rpm for 7 min, and any remnant of dust in the jar surfaces and O-rings was removed prior to the next extraction.

The same procedure was applied for the stainless steel tube with only one difference that is the evacuation and Zero Air flushing and pumping were achieved through a double needle piercing the rubber septum. Blanks, isotopic labelling, and extraction experiments were performed by applying pressures ranging from 10 to 20 MPa with a hydraulic press (Figure 2). A new tube was used for each experiment. The recommendations for optimal analytical conditions, including sample size, sample type, and extraction technique are summarized in section 4.5.

3 Results

3.1 Concentrations

The CO_2 and CH_4 concentrations measured by the Picarro G2201-i in this study depend on the internal pressure of the jar that was kept constant at 210 kPa at the beginning of every experiment, and on the accuracy of the sample dilution in the SSIM2 module. The latter is affected by (i) the amount of gas injected which might vary from one to another injection, and (ii) the additional volume of the inlet line, which was modified for the introduction of gas samples with GC syringes. The concentrations presented in this work do not consider possible changes of volume, temperature and pressure within the jar or tube and should be considered specific for this analytical setup.

3.2 Ball milling

3.2.1 Blank experiments

The change in CH_4 and CO_2 concentrations between the gas measured before and after the milling are hereafter expressed as Equations 1, 2:

$$\Delta CH_4 = CH_{4\,post-mill} - CH_{4\,pre-mill} \quad (1)$$

$$\Delta CO_2 = CO_{2\,post\text{-}mill} - CO_{2\,pre\text{-}mill} \quad (2)$$

Hence, a positive ΔCH_4 implies an increase in CH_4 concentration in the gas phase inside the jar with respect to the initial conditions before the milling. Conversely, a negative ΔCH_4 refers to a decrease in CH_4 concentration in the gas phase inside the jar with respect to the initial conditions before the milling. The uncertainties on the ΔCH_4 and ΔCO_2 values were calculated considering the standard deviation reported by the analyser on the single $CH_{4\,pre\text{-}mill}$ and $CO_{2\,pre\text{-}mill}$ measurements, and the standard deviation calculated on two to three replicated $CH_{4\,post\text{-}mill}$ and $CO_{2\,post\text{-}mill}$ measurements (Supplementary Table S1).

The ΔCH_4 and ΔCO_2 were obtained at different rotation speeds and for three experimental setups: 1) 50 g of Novate granite (CH_4- and CO_2-free) + 3 balls; 2) 3 balls and no mill feed; 3) 50 g of industrial glass +3 balls. The experiments without mill feed were conducted at rotation speeds <200 rpm to avoid damaging the internal jar and balls surface.

The results suggest that the blank levels vary as a function of rotation speed, type of material, and grinding stock filling degree (Figures 4A, B). Experiments with Novate granite and without mill feed produced similar trends with a positive ΔCH_4 which increased with rotation speed. The presence of rock sample in the jar resulted in lower ΔCH_4 for a given rotation speed relative to the experiments without mill feed. These blank experiments produced both positive and negative ΔCO_2 at low rotation speeds. Nevertheless, for rotation speeds >200 rpm, ΔCO_2 was always positive. The experiment with Novate granite at 200 rpm resulted in slightly higher ΔCO_2 (19.0 ppm) compared to the experiment without mill feed (12.8 ppm). Blank experiments with

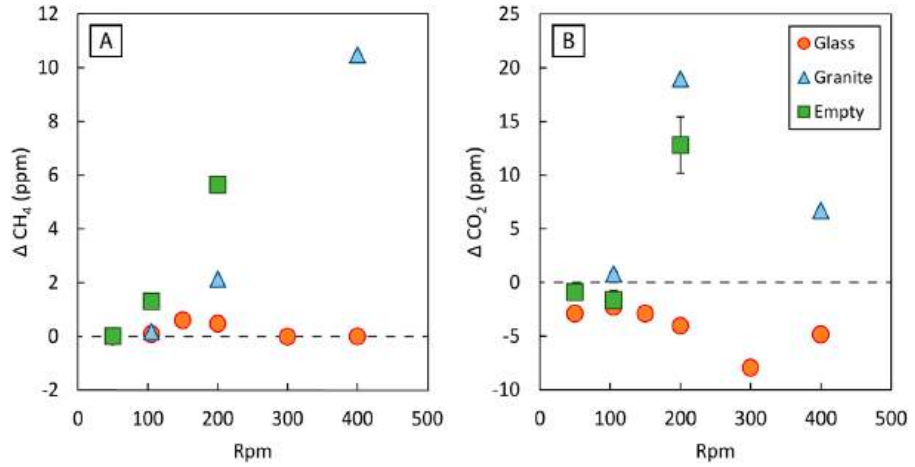

FIGURE 4
The change in CH_4 and CO_2 concentrations (expressed in ppm) as ΔCH_4 **(A)** and ΔCO_2 **(B)** as a function of rotation speed (expressed in rpm). Each point corresponds to the difference between a single pre-mill measurement and an average value calculated based on 2-3 replicated post-mill measurements. The different symbols correspond to the three different analytical setups: 50 g of glass +3 ZrO_2 balls in the jar; 2) 50 g of Novate granite +3 ZrO_2 balls in the jar; 3) 3 ZrO_2 balls in the jar. Error bars that are not visible are smaller than the symbol size.

glass displayed slightly positive ΔCH_4 at 150 rpm and 200 rpm, while at higher speeds no change in CH_4 concentration was detected. All experiments with glass resulted in a negative ΔCO_2 and a weak negative correlation between ΔCO_2 and rotation speed.

The δ^{13}C-CH_4 of the blank gases in experiment with Novate granite and without mill feed varied between −44 and −49‰ in the HP mode and −152 and −228‰ in the HR mode (Supplementary Table S2). Such a difference in between these two values is unexpectedly high and likely reflects the presence of an interferent produced during the experiment. The interference causing high residuals and baseline offsets was indeed identified by the Picarro ChemDetect software. Such effects may be indicative of the presence of heavier hydrocarbons that could not be determined more specifically. Repeated measurements with the GC-TCD technique confirmed the presence of CH_4, CO_2, O_2 and N_2 in the blank experiments, but no other gas species could be detected (Supplementary Figure S9). Therefore, it was not possible to unambiguously determine the cause of the interference. When comparing the blank and the laboratory air chromatograms (normalized to the O_2-N_2 peak intensity to correct for differences in the injected volume), the absolute abundance of CH_4 differs. The gas filling the jar displays higher relative CH_4 abundance compared to the laboratory air (Supplementary Figure S10).

3.2.2 Isotopic labelling

We repeated the experiments after pumping two reference gases (detailed description of the composition in section 2.2) inside the jar at 100 kPa gauge pressure to evaluate changes in concentration and isotopic composition. The changes in δ^{13}C-CH_4 and δ^{13}C-CO_2 between the gas measured before and after a milling cycle are hereafter referred as Equations 3, 4:

$$CH_4\text{: } \Delta^{13}C_{post\text{-}pre} = \delta^{13}C\text{-}CH_{4\,post\text{-}mill} - \delta^{13}C\text{-}CH_{4\,pre\text{-}mill} \quad (3)$$

$$CO_2\text{: } \Delta^{13}C_{post-pre} = \delta^{13}C - CO_{2\,post-mill} - \delta^{13}C - CO_{2\,pre-mill} \quad (4)$$

For instance, a positive $\Delta^{13}C_{post\text{-}pre}$ implies an increase in the $^{13}C/^{12}C$ ratio of CH_4 between the gas sample extracted before and after the milling cycle. The uncertainties on the $\Delta^{13}C_{post\text{-}pre}$ values were calculated considering the standard deviation reported by the analyser on the single $\delta^{13}C_{pre\text{-}mill}$ measurements, and the standard deviation calculated on two to three replicated $\delta^{13}C_{post\text{-}mill}$ measurements when available (Supplementary Tables S4, S5).

A positive ΔCH_4 was calculated for experiment with Novate granite, without mill feed and with glass at 100 rpm, as observed in blank experiments, while a negative ΔCH_4 characterized experiments with glass at 200 and 300 rpm (Figure 5A). A strongly negative ΔCO_2 was detected in all the experiments where the milled material was present in the jar (Figure 5C). The $\Delta^{13}C_{post\text{-}pre}$ of CH_4 in the HP mode, ranged between −1.4 and +1.1‰ in the experiments with Novate granite and without mill feed (Figure 5B), the δ^{13}C-CH_4 fell in the range of the isotopic standard (−44.6‰+/-0.3‰) and the experimentally produced CH_4 (−43 to −49‰). In the HR mode the $\Delta^{13}C_{post\text{-}pre}$ of CH_4 was characterized by extremely negative values in experiments with Novate granite and without mill feed (Supplementary Table S4). These results might reflect the same interference effect noticed in the blank experiments where δ^{13}C-CH_4 in HR mode displayed extremely negative values (−151 to −228‰) with this filling type. A positive $\Delta^{13}C_{post\text{-}pre}$ of CH_4 was observed in experiments with glass where $\Delta^{13}C_{post\text{-}pre}$ increases with rotation speed, up to $\Delta^{13}C_{post\text{-}pre}$ = +10.7‰ at 300 rpm (Figure 5B). Carbon dioxide displayed a negative $\Delta^{13}C_{post\text{-}pre}$ in experiment with Novate granite and without mill feed at 200 rpm (between −1 and −4‰) while in the experiment with glass at 105 rpm, CO_2 displayed a positive $\Delta^{13}C_{post\text{-}pre}$ = +2‰ (Figure 5D). The CO_2 concentration was too low to measure δ^{13}C-CO_2 in experiments with glass at higher rotation speed. The experiment without mill feed at 200 rpm, characterized by the largest interference effect on δ^{13}C-CH_4 in HR mode, featured also the largest uncertainty on δ^{13}C-$CO_{2\,post\text{-}mill}$ measure.

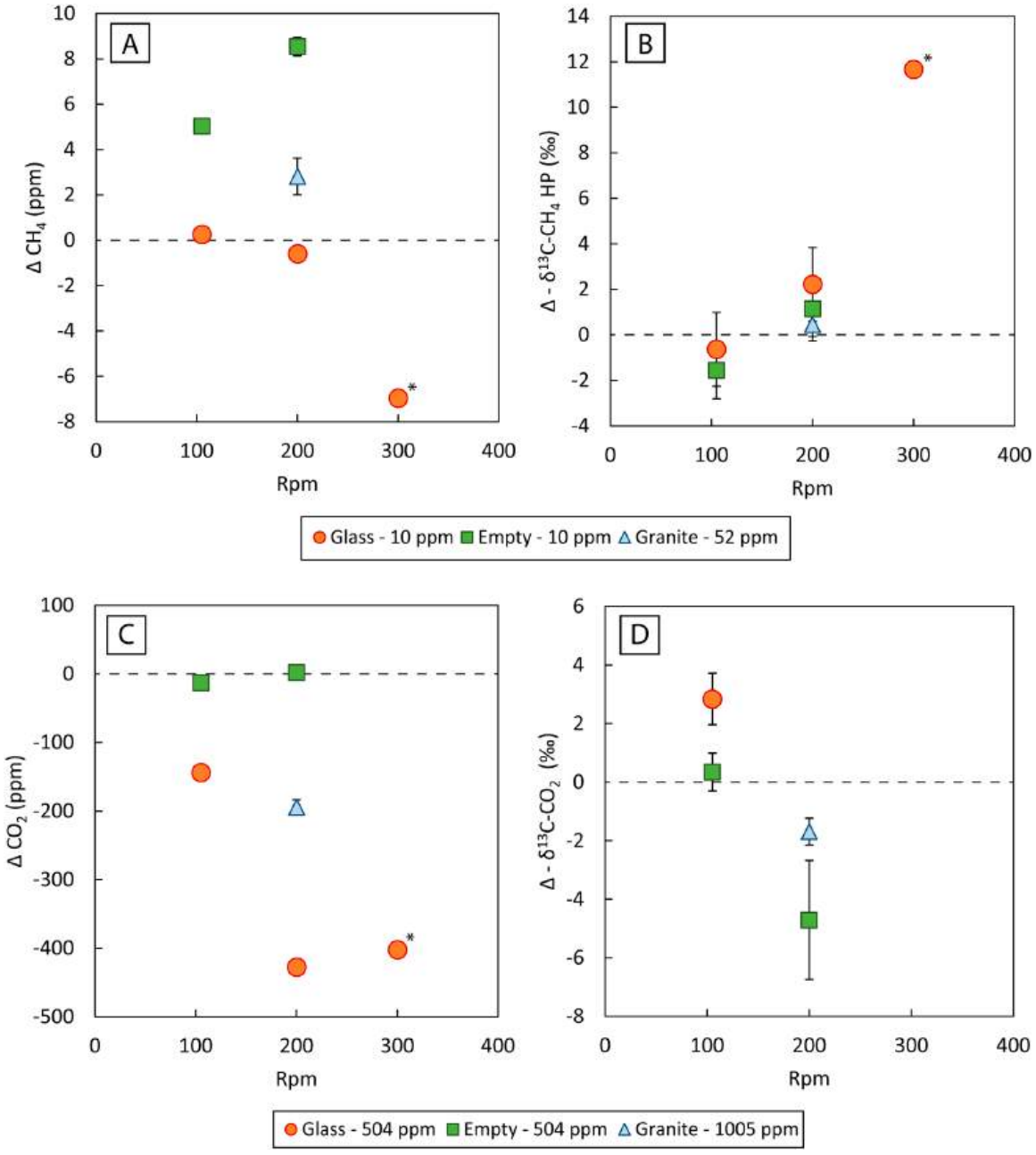

FIGURE 5
Change in CH_4 and CO_2 concentrations after ball milling experiments, expressed as Δ CH_4 **(A)** and Δ CO_2 **(B)** and isotopic composition expressed as $\Delta^{13}C_{post\text{-}pre}$ for CH_4 **(C)** and CO_2 **(D)** as a function of rotation speed (expressed in rpm). Each point corresponds to the difference between a single pre-mill measurement and an average value calculated based on 2-3 replicated post-mill measurements, except for the experiment marked by an asterisk, where a single post-mill measure was available. The different symbols correspond to the three different analytical setups: 50 g of glass +3 ZrO_2 balls in the jar +10 ppm CH_4 – 504 ppm CO_2 standard; 2) 50 g of Novate granite +3 ZrO_2 balls in the jar +50 ppm CH_4 – 1,000 ppm CO_2 standard; 3) 3 ZrO_2 balls in the jar +10 ppm CH_4 – 504 ppm CO_2 standard. Error bars are provided for all experiments except for the one marked by an asterisk. When not visible, the error bars are smaller than the symbol size.

3.3 Tube crushing–blank and isotopic labelling experiments

Following the same procedure described in section 3.2 we performed blank and isotopic labelling experiments on the tube crushing device. The concentrations and carbon isotope ratios of CH_4 and CO_2 in the tube before the crushing experiments are reported in Supplementary Tables S3–S6, respectively.

Crushing an empty stainless steel tube flushed and pumped with Zero Air produced no appreciable changes in CH_4 and CO_2 concentrations (Supplementary Table S3). Similarly, the isotopic labelling test with the crushing device did not produce

10.3389/feart.2024.1438382

TABLE 1 Interlaboratory comparison test results comparing the data obtained in this study with the results of Mangenot et al. (2021) and Boutier et al. (2024). The δ^{13}C-CH_4 values reported from this study are measured in HR mode due to the high CH_4 concentrations (up to 525 ppm) detected by the Picarro G2201-i analyser. Each δ^{13}C-CH_4 value from this study is an average of 2–3 replicated measurements of gas extracted from the jar/tube. The average δ^{13}C-CH_4 was calculated for injections in which the δ^{13}C-CH_4 change reached a steady state.

Sample	Weight (g)	Extraction method	Gas filling	Rotation speed (rpm)	Milling duration (min)	δ^{13}C-CH_4 (‰) CRDS	1σ	δ^{13}C-CH_4 (‰) GC-IRMS	1σ	CH_4 corr. (ppm)	Reference
Val d'Illiez quartz	5 to 35	Crushing electromagnet device	Vacuum					from −28.03 to −29.08		NA	Mangenot et al. (2021)
Val d'Illiez quartz	68	Ball milling	Zero Air	200	3	−27.4	0.1			13,010	This study
Val d'Illiez quartz	55	Ball milling	Zero Air	400	3	−29.9	0.1			6,730	This study
Val d'Illiez quartz	15	Crushing tube	Zero Air	—	—	−26.9	0.7			10,848	This study
V18-2A	20.9	Ball milling	N_2	700	7	−12.7	0.1	−12.93	0.6	NA	Boutier et al. (2024)
V18-2A	83	Ball milling	Zero Air	400	3	−11.8	0.4			2,958	This study
V18-2A	15	Crushing tube	Zero Air	—	—	−11.6	0.3			1,668	This study

any detectable change in either CO_2 and CH_4 concentrations or isotopic compositions compared to the reference gas (Supplementary Table S6). Repeating the experiment with 20 g of Novate granite gravel resulted in a negative δ^{13}C-CH_4 change of 1‰, while no changes in δ^{13}C-CO_2 and CH_4 and CO_2 concentrations were observed relative to the reference gas (Supplementary Table S6).

3.4 Interlaboratory comparison of natural CH_4-bearing samples

Interlaboratory comparison tests were carried out on natural samples hosting CH_4-rich fluid inclusions in quartz crystals coming from the Val d'Illiez (Swiss Alps) (Mangenot et al., 2021) and in a partially serpentinized peridotite coming from the Belvidere Mountain (Vermont) (Boutier et al., 2024) (Section 2.6). The extraction parameters and the results are summarized in Table 1.

Several aliquots of gas were extracted from the jar after each experiment. Considering the high CH_4 concentration in the sample, CH_4 was diluted in Zero Air by injecting between 0.2 and 5 mL of extracted gas into the SSIM2 module. The CH_4 concentration was then corrected for the dilution effect using the following Equation 5:

$$CH_{4\,corr} = CH_{4\,meas} * (SSIM_{vol}/Injected_{vol}) \quad (5)$$

Where $CH_{4\,meas}$ indicates the CH_4 concentration measured by the analyser, $SSIM_{vol}$ the internal volume of the SSIM2 module corresponding to 20 mL and $injected_{vol}$ the volume of sample injected in the SSIM2 module. It is important to remark that the value of $CH_{4\,corr}$ is not corrected for the difference in internal volume between the milling jars and the tubes. Therefore, the $CH_{4\,corr}$ values reported for ball milling and crushing are not directly comparable.

Only the δ^{13}C-CH_4 measured in HR mode is considered in this study due to the high CH_4 concentrations detected by the CRDS analyser despite the dilution in the SSIM2 module.

As shown in Figure 6, the CH_4 concentration and δ^{13}C-CH_4 measured by the isotopic analyser changed through different injections from the jar after a milling cycle: increases in CH_4 concentration and δ^{13}C-CH_4 values were observed after several syringe extractions up to a plateau approaching the values reported by Mangenot et al. (2021) (Supplementary Table S7). The same effect was observed in the experiment with the peridotite sample characterized by Boutier et al. (2024) (Figure 6; Supplementary Table S8) and in the crushing experiments. Therefore, the first 20 mL and 2–10 mL of gas extracted from the jars and the tubes, respectively, were excluded from the average CH_4 concentration and δ^{13}C-CH_4 calculations for all the measurements.

Despite the differences between the extraction apparatuses and the parameters used in this work compared to previous studies, both ball milling and crushing techniques allowed to replicate previously reported δ^{13}C-CH_4 within+/-1‰ (Table 1; Figure 7). Considering the extraction tests on quartz crystals, the milling at 200 rpm and the crushing technique produced higher δ^{13}C-CH_4, −27.4‰ and −26.9‰ respectively, compared to the milling at 400 rpm (−29.9‰) (Table 1; Figure 7). Regarding the test with the peridotite sample, the extraction technique did not affect the measured δ^{13}C-CH_4. Milling

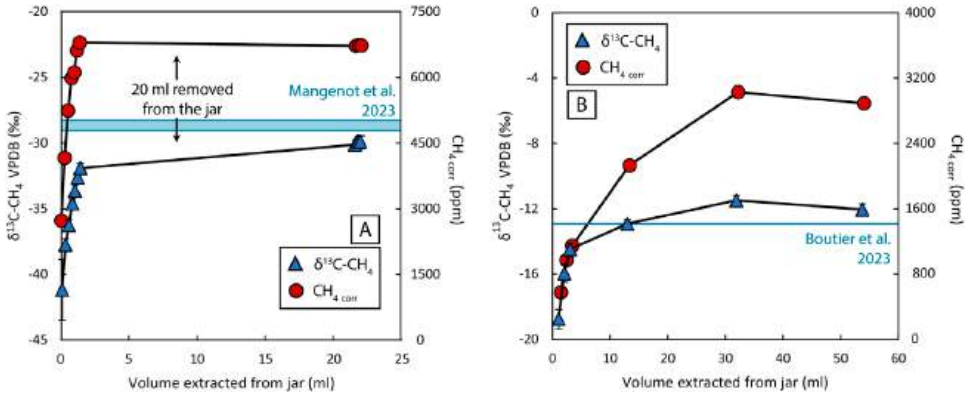

FIGURE 6
CH_4 concentration corrected for dilution (expressed in ppm) in red circles and $\delta^{13}C$-CH_4 VPDB (expressed in ‰) in blue triangles as a function of volume extracted from the jar through a GC syringe after a single milling of cycle (milling duration: 3 min – rotation speed: 400 rpm). **(A)**: experiment with 55 g of Val d'Illiez quartz; **(B)**: experiment with 83 g of V18-2A. Each point represents a single measurement. The light blue rectangles highlight the range of $\delta^{13}C$-CH_4 values measured by Mangenot et al. (2021) and Boutier et al. (2024). When not visible, the $\delta^{13}C$-CH_4 error bars are smaller than the symbol size.

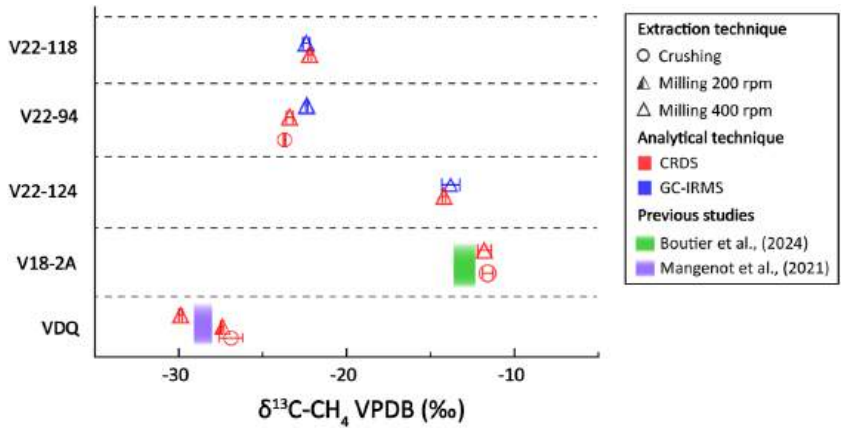

FIGURE 7
$\delta^{13}C$-CH_4 VPDB (expressed in ‰) measured through CRDS, in red, and GC-IRMS, in blue, by ball milling at a rotation speed of 200 rpm, half-filled triangle, and 400 rpm, empty triangle, and by crushing, circle. The $\delta^{13}C$-CH_4 measured for sample V18-2A and Val d'Illiez quartz (VDQ) are compared with values reported in previous studies by Boutier et al. (2024), in green, and Mangenot et al. (2021), in purple.

68 g of Val d'Illiez quartz at 200 rpm released about 13,010 ppm of CH_4, while milling of sample V18-2A at 400 rpm released about 2,958 ppm of CH_4 (Table 1).

3.5 Inter-technique comparison on natural CH_4-bearing samples

The inter-technique comparison between the CRDS and GC-IRMS techniques was performed on one sample of partially serpentinized peridotite and two samples of serpentinites crosscut by carbonate veins coming from the Belvidere Mountain Complex (Supplementary Section S4). The extraction parameters and the results are summarized in Table 2.

The duplicate measurements were performed on different aliquots of the same sample, under a Zero Air atmosphere for CRDS, and under a He atmosphere for GC-IRMS analysis. The CRDS measurements were performed through syringe injection while the gas samples for GC-IRMS analysis were first transferred by expansion to pre-evacuated Pyrex® bottles. The average $\delta^{13}C$-CH_4 values resulting from the CRDS analysis were calculated as described in Section 3.4, excluding the first 20 mL of gas extracted from the jar.

The comparison between the CRDS and the GC-IRMS techniques shows good reproducibility of the $\delta^{13}C$-CH_4 values for duplicate analysis of the same sample with variations of $\delta^{13}C$-CH_4 ranging between 1.3‰ and 0.2‰ over three different samples (Figure 7). Therefore, the precision of the inter-technique comparison experiments falls within the $\delta^{13}C$-CH_4 analytical precision, <0.3‰ in the CRDS setup, or displays minor offsets up to 1.0‰. Overall, the $\delta^{13}C$-CH_4 is independent of the sampling technique–i.e.: syringe injection

TABLE 2 The results of the inter-technique comparison test carried out at 400 rpm with a milling duration of 3 min. The table shows the $\delta^{13}C\text{-}CH_4$ VPDB, expressed in ‰, measured through CRDS and GC-IRMS analysis on different aliquots of the same sample. The CH_4 concentrations corrected for the dilution effect in the SSIM2 are additionally reported in ppm.

Sample	Lithology	Weight (g)	Extraction method	Rotation speed (rpm)	Milling duration (min)	Gas filling	Sampling method	Analytical technique	$\delta^{13}C\text{-}CH_4$ VPDB (‰)	1σ	$CH_{4\ corr.}$ (ppm)
V22-118	Carbonate veins in serpentinite	110	Ball milling	400	3	Zero Air	Syringe	CRDS	−22.2	0.1	67
V22-118	Carbonate veins in serpentinite	109	Ball milling	400	3	He	Expansion	GC-IRMS	−22.4	0.2	—
V22-94	Carbonate veins in serpentinite	101	Ball milling	400	3	Zero Air	Syringe	CRDS	−23.4	0.2	23,630
V22-94	Carbonate veins in serpentinite	101	Ball milling	400	3	He	Expansion	GC-IRMS	−22.4	0.1	—
V22-94	Carbonate veins in serpentinite	22	Crushing tube	—		Zero Air	Syringe	CRDS	−23.7	0.1	19,853
V22-124	Partially serp. peridotite	72	Ball milling	400	3	Zero Air	Syringe	CRDS	−14.2	0.1	285
V22-124	Partially serp. peridotite	113	Ball milling	400	3	He	Expansion	GC-IRMS	−13.8	0.5	—

10.3389/feart.2024.1438382

vs. expansion to a bottle, and of the jar atmosphere–i.e.: Zero Air vs. He.

The CH_4 concentrations in the analysed gases can vary significantly depending on the sample. Milling 101 g of carbonate veins rich in fluid inclusions from sample V22-94, yielded a CH_4 concentration of 23,630 ppm (Table 2). On the other hand, milling 110 g of sample V22-118, poor in carbonate-hosted fluid inclusions, yielded a significantly lower CH_4 concentration of 67 ppm (Table 2). Despite this large difference in CH_4 concentration, fluid inclusions released from carbonate veins in both samples yielded overlapping $\delta^{13}C$-CH_4 values (Figure 7). Even though Etiope et al. (2018) reported high CO_2 concentrations when ball milling carbonate-rich samples, no increase in CO_2 concentration was detected after milling samples V22–94 and V22-118. Milling 72 g of partially serpentinized peridotite from the same locality yielded a CH_4 concentration of 285 ppm and heavier $\delta^{13}C$-CH_4, ranging between −13.8 and −14.2‰. For comparison, olivine-hosted fluid inclusions from sample V18-2A, coming from the same locality, display similar $\delta^{13}C$-CH_4, ranging between −12.9 and −11.6‰.

3.6 Comparison with fluid inclusion-poor samples

Three serpentinized peridotite samples, poor in fluid inclusions, were selected to test the reproducibility of the $\delta^{13}C$-CH_4 measurements at low CH_4 concentrations. Milling between 106 and 113 g of peridotite at 400 rpm yielded CH_4 concentrations varying between 23.56 ppm and 31.78 ppm (Table 3) which are 2–3 orders of magnitude lower than the CH_4 concentrations detected for samples in the interlaboratory comparison test (Table 1). At these low concentrations, background CH_4 might represent a significant fraction of the analysed gas phase, offsetting the $\delta^{13}C$-CH_4 of natural samples. To evaluate these effects, split samples were also analysed by crushing in stainless-steel tubes. The $\delta^{13}C$-CH_4 values measured with the two extraction techniques differ slightly for a given sample (see Table 3). Milling samples V22-45 and V22-80 resulted in lower $\delta^{13}C$-CH_4 (2‰ and 4‰ in difference, respectively) compared to the gases extracted by crushing the same samples. The crushing experiment with sample V22-78 produced extremely small concentrations of CH_4 and lower $\delta^{13}C$-CH_4 compared to the milling experiment. The latter result might suggest mixing with atmospheric CH_4. An increase in air contamination (CO_2 and H_2O concentration) in the tubes was observed after extracting approximately 10–20 mL of gas from the crushed tubes.

4 Discussion

4.1 Parameters controlling blank yields in the ball milling technique

Our results highlight complex changes in blank CO_2 and CH_4 yields as a function of three milling parameters: rotation speed, grinding stock filling degree and type of filling material. These parameters are discussed separately.

4.1.1 Rotation speed effect

Rotation speed seems to play a major role in the production of CH_4 and CO_2 in blank experiments (Figures 4A, B) as suggested in previous studies (Etiope et al., 2018). Increasing rotation speed leads to an increase in blank levels in both experiments with rock filling and without mill feed in the jar (Figures 4A, B). Experiments that produced the greatest blank yields actually show strong interference in the absorbance bands of CO_2 and CH_4 in High-Range mode and high residuals and baseline offsets. This suggests the production of an unidentified molecule, possibly heavier hydrocarbons, affecting the measurements. It has been demonstrated that increasing rotation speed generates higher temperatures inside ball mills (Schmidt et al., 2016) and favours mechanochemically driven reactions (Li et al., 2023; Sawama et al., 2020). This correlation advocates for a link between the energy generated mechanically by the milling balls impacts and the blank production of CH_4 and CO_2. Similar results were observed by Welhan (1988) and Etiope et al. (2018) in stainless steel crushers where increasing milling duration led to higher CH_4 blank levels. It has been proposed that carbon-bearing impurities in stainless-steel can combine with hydrogen atoms to produce CH_4 during metal-metal friction (Higaki et al., 2006). If trace amounts of carbon are present in the ZrO_2 jar and/or milling balls a similar mechanism could explain our blank CH_4 yields (Figure 4A). The O-rings present on the jar lid might represent another possible source of carbon in the extraction apparatus.

Another explanation for the blank production of CH_4 could be the presence of carbon-bearing contaminants introduced in the jars during the experiments or persisting after cleaning of the extraction apparatus. Nonetheless, in the latter case, we would see variability in blank CH_4 yields from one experiment to another, whereas our results show that the blank yields were homogeneous through time, replicable, and dependent only on rotation speed and filling material (Supplementary Table S1). Traces of condensed organic matter in rocks, like the Novate granite, could represent another possible source of contamination. At high temperatures organic matter can crack to generate artificial thermogenic CH_4. This process can be particularly problematic in thermal decrepitation (Grozeva et al., 2020), nevertheless the current data do not allow to constrain the temperatures reached during ball milling in our experiments.

Alternatively, it has been demonstrated that in the presence of CO_2 and H_2O, ball milling can generate CH_4 through mechanically induced methanation of CO_2 (Sawama et al., 2020). This type of reaction might take place at the expense of CO_2 and H_2O that remained adsorbed on the jar and balls surfaces after the evacuation and flushing stages. This is unlikely, since at fixed milling parameters and jar filling, longer evacuation times (2 h vs 21 h) produced no change in blank CH_4 yields (Supplementary Table S1). Mechanochemical methanation of CO_2 could be also linked to the generation of H_2 during milling of silicate-bearing rocks–like the Novate granite - in the presence of H_2O (Sugisaki et al., 1983).

4.1.2 Grinding stock filling degree effect

The increase in grinding stock filling degree, represented in this study by the comparison between experiments without mill feed and with Novate granite, resulted in lower CH_4 blank levels

TABLE 3 The comparison between ball milling and crushing a sealed stainless steel tube with a hydraulic press with samples of partially serpentinized peridotite hosting a small number of CH_4-rich fluid inclusions. The $\delta^{13}C$-CH_4 values reported from this study are measured in HP mode due to the low CH_4 concentrations (between 2 and 25 ppm) detected by the Picarro G2201-i analyser. Experiments for which a standard deviation is reported are an average of 2–3 replicated measurements of gas extracted from the jar/tube. Experiments lacking standard deviation are the result of a single measurement. The average $\delta^{13}C$-CH_4 was calculated for injections in which the $\delta^{13}C$-CH_4 change reached a steady state. $\delta^{13}C$-CH_4.

Sample	Lithology	Weight (g)	Extraction method	Rotation speed (rpm)	Milling duration (min)	$CH_{4\ corr.}$ (ppm)	1σ	$\delta^{13}C$-CH_4 VPDB (‰)	1σ
V22-45	Strongly serp. peridotite	106	Ball milling	400	3	31.78	NA	−20.1	NA
V22-45	Strongly serp. peridotite	15	Crushing tube	—		14.94	1.54	−18.1[a]	0.1
V22-78	Strongly serp. peridotite	110	Ball milling	400	3	23.19	0.03	−19.6	0.1
V22-78	Strongly serp. peridotite	15	Crushing tube	—		2.65	NA	−21.6[b]	NA
V22-80	Strongly serp. peridotite	113	Ball milling	400	3	25.62	0.03	−19.6	0.1
V22-80	Strongly serp. peridotite	15	Crushing tube	—		8.67	0.17	−15.6[a]	0.5

[a]Highlights values unaffected by isotopic fractionation or mixing with blank CH_4. $\delta^{13}C$-CH_4.
[b]Highlights value affected by atmospheric contamination.

(Figure 4A) and lower interference in the HR mode. These results agree with previous studies carried out with stainless steel extraction apparatuses (Etiope et al., 2018; Grozeva et al., 2020; Welhan, 1988), where increasing the volumetric ratio between the sample and the extraction apparatus resulted in lower blank levels. It has been demonstrated that increasing the grinding stock filling degree reduces the milling bed temperature (Schmidt et al., 2016) due to the decrease of the milling balls speed and path. Moreover, the grinding stock acts as a heat sink as energy is dissipated in more material (Schmidt et al., 2016).

Alternatively, adsorption of blank-generated CH_4 onto rock powder might result in apparent lower blank levels (Welhan, 1988). The latter hypothesis will be discussed in greater detail in section 4.2. Milling Novate granite at 200 rpm resulted in higher CO_2 blank yields compared to experiment without mill feed (Figure 4B). This difference might be related to the presence of small amounts of CO_2 in the Novate granite fluid inclusions that could not be detected through Raman spectroscopy. Although natural untreated materials are often used in blank experiments (Etiope et al., 2018; Salvi and Williams-Jones, 2003; Sanz-Robinson et al., 2021), such data call for caution in their use for blank evaluation.

The 250 mL ZrO_2 jars used in this study allowed to load up to 100–110 g of partially serpentinized peridotite samples cut into 6-mm thick slices, in order to maximize the grinding stock filling degree and minimize the frictional heating. For reference, considering a density of the serpentinized peridotite ranging between 2.6 and 2.9 g/cm^3, the optimal grinding stock volume for the ball milling technique ranges between 34 and 37 cm^3 of rock sample, corresponding to 13%–14% of the internal jar volume. Considering this volumetric ratio as the optimal condition to minimize frictional heating, a jar with an internal volume of 50 mL should allow to reduce the sample size to 8 cm^3, corresponding to 18–20 g of partially serpentinized peridotite. Nevertheless, it is highlighted that smaller jar volumes may result in too high dilution effects if the adopted analytical protocol uses a Picarro SSIM2.

4.1.3 Type of filling

Very large discrepancies are observed when comparing the CO_2 and CH_4 blank yields between different types of filling: experiments with glass display significantly lower blank levels compared to experiments with Novate granite (Figures 4A, B). Rosenkranz et al. (2011) observed significant differences in the ball motion of milling balls depending on the type of filling present in the ball mill. These authors observed the formation of a mill feed coating on the milling balls causing changes in the friction conditions during the comminution process (Rosenkranz et al., 2011). Therefore, it could be possible that large variations in blank CO_2 and CH_4 yields might depend on the type of rock/filling material used in the experiments. Alternatively, the large differences in blank levels might arise from the interaction between CO_2 and CH_4 molecules and new fresh, chemically active surfaces generated during the milling process.

Another factor that should be carefully evaluated prior to any fluid inclusion carbon isotope analysis is the presence of carbon-rich solid phases, which could lead to blank CH_4 and/or CO_2 production when exposed to heat generated by frictional heating. For instance, Li et al. (2023) reported CH_4 generation through mechanochemical hydrogenation of carbon substrates (such as PET, anthracite, coal, and active carbon) using ball milling. Similarly, Etiope et al. (2018) reported higher CO_2 concentrations and $\delta^{13}C$-CO_2 values in ball milling experiments with limestone compared to experiments with granite, and quartz, pointing to CO_2 input from calcite.

4.2 Adsorption

One of the main disadvantages of mechanical extraction techniques is the adsorption of the extracted gases onto newly formed chemically active surfaces (Barker and Torkelson, 1975; Norman and Sawkins, 1987; Welhan, 1988), causing lower extraction efficiency and potentially leading to isotopic fractionation effects. Some of the trends observed in the isotopic labelling results might result from adsorption processes. For instance, the decrease in CO_2 concentration in all the experiments where a gas standard was stored in the jar together with freshly generated glass or rock powder (Figure 5C) might be caused by CO_2 adsorption. The magnitude of CO_2 concentration decrease changed dramatically with rotation speed. For instance, in the presence of a glass powder produced at 105 rpm, only 30% of the CO_2 pumped in the jar was recovered, while for a glass powder produced at 200 rpm only 2% was recovered. This trend could be consistent with the adsorption process since increasing rotation speed causes a decrease the grain size of the powder and, therefore, an increase in the powder surface area. The extent of CO_2 concentration decrease varied considerably depending on the nature of the jar filling: for a rotation speed of 200 rpm, the magnitude of CO_2 adsorption is approximately twice as strong on glass powder as on Novate granite powder (Figure 5C). This may be explained by different adsorption properties among materials (Kalinkin et al., 2002; Rigopoulos et al., 2018; Welhan, 1988).

Changes in CH_4 concentration were more complex and dependent on the nature of the filling phase. For instance, CH_4 concentration decreased only in experiments with glass at 200 and 300 rpm (Figure 5A) suggesting that this type of material, compared to granite powder, might potentially favour CH_4 adsorption. This hypothesis would explain the generally lower blank CH_4 yields in experiments with glass (Figure 5A). In general, these results are consistent with previous works that showed that CO_2 is more easily adsorbed than CH_4 and that silica-rich powder favours CH_4 adsorption (Barker and Torkelson, 1975; Welhan, 1988). Considering the large variety of rock types and minerals that can host fluid inclusions and their different mechanical properties, a more comprehensive study would be needed to better understand CO_2 and CH_4 interactions with the surfaces of different rock powders.

4.3 Syringe sampling effect

The increase in CH_4 concentration and $\delta^{13}C\text{-}CH_4$ observed after several syringe extractions from the same jar after a single milling cycle (Figure 6) bears strong similarities with the trends observed in CH_4 diffusion experiments through porous materials (Zhang and Krooss, 2001) where the lighter $^{12}CH_4$, displaying faster diffusivity compared to $^{13}CH_4$, is enriched in the diffusion front generating a depletion in $\delta^{13}C\text{-}CH_4$ in the first time of the experiment. The process occurring in the jar and in the tubes instead of being driven by time seems to be controlled by the extracted volume: the first 20 mL of gas extracted from the jar display lower $\delta^{13}C\text{-}CH_4$ approaching a steady value of $\delta^{13}C\text{-}CH_4$ after several extractions. Therefore, the observed trends might reflect a diffusion isotopic fractionation process occurring in the jar during CH_4 migration from the freshly opened inclusions towards the rubber septum. This process could result in a heterogeneous distribution of CH_4 in the jar/tube after the milling/crushing experiments with the development of a diffusive front depleted in $^{13}CH_4$. Our results suggest that progressive removal of gas with the syringe drives homogenization of CH_4 inside the jar/tube.

Alternatively, these analytical artifacts might be a result of the gas sampling technique with the GC syringes adopted in this study, which are not equipped with valves. A leak of gas from the GC syringes when the jar has an internal overpressure could explain the increase in CH_4 concentration observed after several extractions, as the gas pressure in the jar decreases. Nevertheless, it is difficult to explain the changes in $^{13}C/^{12}C$ ratio with this mechanism, since during the diffusion process the CH_4 fraction remaining in the syringe should display heavier $\delta^{13}C\text{-}CH_4$.

Overall, the comparison between results collected through syringe injections and gas transferred to Pyrex® bottles show minimum differences in $\delta^{13}C\text{-}CH_4$, up to 1‰ (Figure 6). This indicates that, excluding the initial 20 mL of gas from the analysis, gas sampling with GC syringes does not notably impact the measured $\delta^{13}C\text{-}CH_4$ values.

4.4 Evaluating isotopic integrity

The preservation of CH_4 and CO_2 carbon isotope signatures during their extraction from fluid inclusions is not a straightforward process. However, to our knowledge, very few works have yet reported isotopic labelling experiments (Sanz-Robinson et al., 2021) or interlaboratory comparisons (Etiope et al., 2018; Luciani et al., 2022; Potter and Longstaffe, 2007) to evaluate the isotopic integrity of CO_2 and CH_4 carbon isotopic composition after the extraction. The isotopic labelling experiments with Novate granite and without mill feed in the 10–52 ppm concentration range and 105–200 rpm rotation speed range showed good reproducibility of $\delta^{13}C\text{-}CH_4$ (within+/-2‰) in HP mode, whereas $\delta^{13}C\text{-}CH_4$ in HR mode and $\delta^{13}C\text{-}CO_2$ displayed larger offsets up to −50.9‰ and −4.2‰, respectively (Figures 5B, D; Supplementary Tables S4, S5). These offsets could be caused by the presence of other molecules produced during the milling and causing cross-interference with the absorbance bands of CO_2 and CH_4 in HR mode. Nonetheless, it was not possible to unambiguously determine the origin of this interference. It is important to notice that the isotopic composition of blank generated CH_4 (−42 to −48‰) overlaps with the composition of the reference gas (−44.6‰), which hampers the evaluation of mixing between the reference gas and the artificially generated molecules.

The most remarkable changes in $\delta^{13}C\text{-}CH_4$ were observed in experiments with glass, which show an increase in $\delta^{13}C\text{-}CH_4$ up to 10.7‰ at 300 rpm (Figure 5B). The increase in $^{13}C/^{12}C$ ratio was coupled with a decrease in CH_4 concentration. Li et al. (2022a) showed that diffusive loss of CH_4 from poorly sealed bottles causes an increase in $\delta^{13}C\text{-}CH_4$ through time. This process might explain the changes observed in the experiment with glass but fails to explain all the other experiments in which a CH_4 increase was observed after milling. Since the same jars were used for all the tests presented in this study it is unlikely that CH_4 leakage is the cause of the observed trends.

An alternative explanation could be the partial oxidation of CH_4 catalyzed mechanically by ball milling. The oxidation process would drive the remaining CH_4 towards heavier compositions (Kueter et al., 2020). It has been shown that yttria-stabilized-zirconia (YSZ) is a promising material for methane oxidation at high temperatures (>767 °C) (Kogler et al., 2014). Nevertheless, the current data do not allow to constrain the temperature reached during the milling in our experiments. The decrease in CO_2 concentration observed in the experiments with glass also does not support this hypothesis even though we did not evaluate the production of other common by-products of this reaction like graphite and CO (Kueter et al., 2020). In addition, the comparison between replicated measurements performed through milling under a Zero Air atmosphere or milling under a He atmosphere resulted in minor δ^{13}C-CH_4 differences, up to 1‰, suggesting that the presence or lack of O_2 in the jar atmosphere had a minor effect on the analysis.

Another potential interpretation of the observed trends could be isotopic re-equilibration between CO_2 and CH_4 on mineral surfaces favored by increasing temperature at high rotation speeds. Nevertheless, most of the available experimental works (Horita, 2001; Kueter et al., 2019; Sackett and Chung, 1979; Sackett and Conkright, 1997) suggest that the presence of silicate surfaces is insufficient to re-equilibrate CO_2 and CH_4 and that metal catalysts are required. Additionally, CH_4 could interact and/or re-equilibrate with H_2O extracted from the fluid inclusions or adsorbed to the jar walls or milling balls. These processes were investigated in previous mechanical extraction studies (Sanz-Robinson et al., 2021) and showed no relevant effects on the δ^{13}C-CH_4 value. Even though we did not examine this topic in detail, the interlaboratory comparison test on quartz crystals hosting both CH_4 and H_2O-bearing fluid inclusions (see Mangenot et al., 2021) allowed to reproduce previously reported δ^{13}C-CH_4 within+/-1‰ suggesting no significant effect of H_2O on the $^{13}C/^{12}C$ ratio of CH_4.

Alternatively, the observed trends might be related to adsorption of CH_4 onto glass powder. Despite the effects of adsorption on CH_4 isotopic composition are still poorly understood, some studies suggest preferential $^{12}CH_4$ adsorption in the presence of solid substrates (Fuex, 1980; Gunter and Gleason, 1971; Kettel, 1996; Liu et al., 2020). However, it is not clear whether this process alone could explain the magnitude of isotopic fractionation observed in this study. The coupling between adsorption and diffusion could explain the large variation observed in δ^{13}C-CH_4. A decrease in CH_4 in the free gas phase coupled to an increase in adsorbed CH_4 is expected to favour diffusion processes causing an exponential decrease in the amount of CH_4 degassed and increase in δ^{13}C-CH_4 (Li et al., 2022b).

To summarize, the results of the isotopic labelling experiment with the ball milling technique in the concentration range 10 and 50 ppm of CH_4 and 500 and 1,000 ppm CO_2 highlighted complex changes in CO_2 and CH_4 concentrations and carbon isotopic compositions that are challenging to interpret. The largest isotope fractionation effects were observed at low CH_4 concentrations – 10 ppm – and in experiments with synthetic glass.

The results of the interlaboratory comparison experiment suggest that independently of the mechanical extraction technique, the protocols presented in this study allowed to replicate previously reported δ^{13}C-CH_4 values within+/-1‰ for CH_4 concentrations in the range of 1,000–10,000 ppm of CH_4. The CH_4 concentrations measured in these tests were 2–3 orders of magnitude higher than the blanks (Table 1). The crushing technique involves lower energy transfer over a short time period compared to ball milling and it does not generate detectable amounts of CO_2 or CH_4. Moreover, isotopic labelling experiments suggest that CO_2 and CH_4 concentrations and carbon isotopic compositions are not affected by secondary processes, like adsorption, for CH_4 and CO_2 concentrations of 50 ppm and 1,000 ppm respectively. Nevertheless, the stainless steel tubes host smaller volumes of gas compared to milling jars and are more sensitive to air contamination when volumes larger than 10–20 mL are extracted with GC syringes (Section 3.6).

The comparison of the two extraction techniques on split samples hosting small amounts of CH_4-bearing fluid inclusions, and CH_4 concentrations in the range of 20–30 ppm, highlighted differences up to 4‰ in the measured δ^{13}C-CH_4 values (Section 3.6). These discrepancies could be the result of mixing between the CH_4 extracted from the inclusions and the blank CH_4 generated by the milling process (Section 3.2.1).

Even though ball milling is sensitive to analytical artifacts at low CH_4 concentrations, between 10 and 50 ppm, the replicate analyses performed on two different subsets of the same sample showed good reproducibility with small δ^{13}C-CH_4 changes up to 1‰ (Figure 7; Table 2). In addition, the changes in δ^{13}C-CH_4 observed in a range of concentrations varying between 67 and 23,630 ppm appear to be closely related to the mineralogy of the host mineral–olivine in V18-2A and V22-124 and carbonate in V22–94 and V22-118 – and the presence of specific generations of fluid inclusions instead of being controlled by the CH_4 concentration (Table 1, 2, Supplementary Section S5).

Although the CRDS technique allows fast and accurate analysis of CH_4 and CO_2 isotopic composition without separation, it is important to consider the presence of potential interferents present in natural samples that could affect the carbon isotopic composition measured by the analyser. For instance, Rella et al. (2015) reported a variety of species that have cross-interferences with the CH_4 absorbance spectrum, affecting the δ^{13}C-CH_4 measured by a Picarro G2132-i. For instance, H_2S, NH_3, C_2H_6 and C_2H_4 are known to cause distortions of the measured CH_4 absorption spectrum (Rella et al., 2015). The magnitude of this effect varies depending on the molecule and it is proportional to the mole fraction of the contaminant species, and inversely proportional to the CH_4 concentration (Rella et al., 2015). The interlaboratory and inter-technique experiments presented in this study showed good reproducibility between CRDS and GC-IRMS results, suggesting that cross-interference effects, if present, were not significant on the measurement of δ^{13}C-CH_4 of the natural fluid inclusions analyzed in the present work.

Though on-line extraction is generally preferred to off-line systems due to lower detection limits (Salvi and Williams-Jones, 2003), the off-line protocols that we developed provided accurate and replicable measurements of natural samples hosting small CH_4 concentrations, down to 10 ppm of CH_4 (Section 3.6). The extraction protocols developed throughout this research may be potentially extended to the measurement of δD-CH_4 and δ^{18}O-CO_2. Furthermore, large extraction apparatuses (Sanz-Robinson et al., 2021), like the ball milling system designed in this work (Section 2.1), allow to maximize the sample size (up to 207 cm^3) providing large volumes of analyte. This is a

prerequisite for the recently developed CH_4 clumped isotopes ($^{13}CH_3D$ and $^{12}CH_2D_2$) measurements (Gonzalez et al., 2019; Mangenot et al., 2021; Ono et al., 2014; Sanz-Robinson et al., 2021; Young et al., 2017), which can provide unique insights into CH_4-forming processes (Douglas et al., 2017; Mangenot et al., 2021; Stolper et al., 2018; Young et al., 2017).

4.5 Recommendations for fluid inclusion extraction

The protocols developed in this study provide simple and fast means to accurately measure bulk CH_4 and CO_2 concentrations and carbon isotopic composition in natural fluid inclusions. However, some precautions are needed in order to avoid analytical artifacts that could preclude the preservation of CH_4 and CO_2 isotopic composition:

- The crushing technique should be preferred for samples with low CH_4 concentrations, in the range of 10 ppm–50 ppm of CH_4 and for samples with CO_2 concentrations in the range of 1,000 ppm;
- At high concentrations, in the range 3,000 ppm of CH_4, both the crushing and the ball milling techniques allow accurate $\delta^{13}C$-CH_4 measurements (within+/-1‰);
- At lower concentrations, the validity of the ball milling technique should be verified independently. We suggest comparing the two extraction techniques on split samples or monitoring changes in $\delta^{13}C$-CH_4 values as a function of CH_4 concentration on large datasets to distinguish values affected by analytical artifacts;
- The blank production CH_4 and CO_2 generated by ball milling can be minimized by increasing the volume of rock sample in the jar. Optimal conditions for a 250 mL jar can be reached with approximately 100 g of rock sample, corresponding to 13%–14% of the internal jar volume.
- In the presence of carbon-rich solids (e.g.: carbonates, organic matter), the crushing technique should be preferred to minimize blank CO_2 and CH_4 production through frictional heating.

5 Conclusion

This study allowed to evaluate the relative benefits and drawbacks of two off-line mechanical extraction techniques, namely ball milling and crushing in stainless steel tubes, for the extraction of CH_4 and CO_2 hosted in natural fluid inclusions. We combined these techniques with a Cavity Ring-Down Spectroscopy (CRDS) analyser (Picarro G2201-i) allowing accurate CH_4 and CO_2 concentration and $\delta^{13}C$ isotopic composition measurement without gas separation.

We carried out a detailed characterization of potential analytical artifacts through blanks and isotopic labelling experiments. The results suggest that for ball milling, rotation speed, grinding stock filling degree, and filling type are the main parameters controlling changes in CH_4 and CO_2 concentration and $\delta^{13}C$ isotopic composition. Therefore, these factors should be considered when performing fluid inclusions extraction with ball milling.

To overcome the main limitations of ball milling (large volumes of sample required, blank CH_4 and CO_2), alternative mechanical extraction techniques may be adopted, as they seem to limit the development of experimental artifacts. For instance, the crushing technique tested in this work did not generate detectable blank levels of CH_4 and CO_2 and requires smaller sample volumes.

The protocols that we developed allowed to replicate previously measured $\delta^{13}C$-CH_4 values within+/-1‰ and can be applied on gas samples with CH_4 and CO_2 concentrations above 10 and 1,000 ppm respectively. The inter-technique comparison between CRDS and GC-IRMS showed good reproducibility of the $\delta^{13}C$-CH_4 values within+/-1‰ suggesting the lack of cross-interference effects on the CRDS analysis on the studied samples.

The extraction apparatuses designed in this study are versatile and can easily be combined with different analytical techniques, like CRDS, GC-MS or be used to prepare bottles of gas samples. Moreover, the large volume of the ball milling jars gives the opportunity to extract large volumes of analyte, making it potentially suitable for CH_4 clumped isotopes ($^{13}CH_3D$ and $^{12}CH_2D_2$) measurements (Gonzalez et al., 2019; Mangenot et al., 2021; Ono et al., 2014; Young et al., 2017).

Data availability statement

The original contributions presented in the study are included in the article/Supplementary Material, further inquiries can be directed to the corresponding author/s.

Author contributions

OO: Conceptualization, Data curation, Investigation, Methodology, Validation, Visualization, Writing–original draft, Formal Analysis. VM: Investigation, Methodology, Supervision, Visualization, Writing–review and editing, Formal Analysis. SC: Formal Analysis, Investigation, Methodology, Supervision, Writing–review and editing. OS: Methodology, Supervision, Writing–review and editing. ID: Investigation, Supervision, Writing–review and editing, Formal Analysis, Methodology. JF: Supervision, Writing–review and editing. AB: Conceptualization, Funding acquisition, Investigation, Methodology, Project administration, Resources, Supervision, Writing–original draft, Writing–review and editing.

Funding

The author(s) declare that financial support was received for the research, authorship, and/or publication of this article. This work is part of a project that has received funding from the European Research Council (ERC) under the European Union's Horizon 2020 research and innovation programme (Grant agreement No. 864045). A MUR FARE (Grant No. R20ZJYMPAR acronym DRYNK) grant and MUR PRIN 2022 (Grant No. 20224YR3AZ; acronym HYDECARB) to AVB are also acknowledged.

Acknowledgments

We thank S. Hofmann, S. Giordani, A. G. Rombolà, I. Martinez, and A. Calafato for discussion and technical support. We also thank J. Osenda for providing samples of Val d'Illiez quartz. Constructive comments provided by the reviewers Stéphane Affolter, and Tobias Fusswinkel significantly improved the manuscript and were greatly appreciated. Carmen Sanchez Valle is thanked for editorial handling of the manuscript.

Conflict of interest

The authors declare that the research was conducted in the absence of any commercial or financial relationships that could be construed as a potential conflict of interest.

Publisher's note

All claims expressed in this article are solely those of the authors and do not necessarily represent those of their affiliated organizations, or those of the publisher, the editors and the reviewers. Any product that may be evaluated in this article, or claim that may be made by its manufacturer, is not guaranteed or endorsed by the publisher.

Supplementary Material

The Supplementary Material for this article can be found online at: https://www.frontiersin.org/articles/10.3389/feart.2024.1438382/full#supplementary-material

References

Abell, P. I., Draffan, C. H., Eglinton, G., Hayes, J. M., Maxwell, J. R., and Pillinger, C. T. (1970). "Organic analysis of the returned Apollo 11 lunar sample," in Presented at the Apollo 11 Lunar Science Conference, HOUSTON, TX.

Affolter, S., Fleitmann, D., and Leuenberger, M. (2014). New online method for water isotope analysis of speleothem fluid inclusions using laser absorption spectroscopy (WS-CRDS). *Clim. Past* 10, 1291–1304. doi:10.5194/cp-10-1291-2014

Andersen, T., and Neumann, E. R. (2001). Fluid inclusions in mantle xenoliths. Lithos, fluid inclusions: phase relationships - methods - applications. *A Special Issue honour Jacques Touret* 55, 301–320. doi:10.1016/S0024-4937(00)00049-9

Andrawes, F. F., and Gibson, E. K. (1979). Release and analysis of gases from geological samples. *Am. Mineralogist* 64, 453–463.

Andreani, M., Montagnac, G., Fellah, C., Hao, J., Vandier, F., Daniel, I., et al. (2023). The rocky road to organics needs drying. *Nat. Commun.* 14, 347. doi:10.1038/s41467-023-36038-6

Arai, S., Ishimaru, S., and Mizukami, T. (2012). Methane and propane micro-inclusions in olivine in titanoclinohumite-bearing dunites from the Sanbagawa high-P metamorphic belt, Japan: hydrocarbon activity in a subduction zone and Ti mobility. *Earth Planet. Sci. Lett.* 353–354, 1–11. doi:10.1016/j.epsl.2012.07.043

Arakawa, M., Yamamoto, J., and Kagi, H. (2007). Developing micro-Raman mass spectrometry for measuring carbon isotopic composition of carbon dioxide. *Appl. Spectrosc.* 61, 701–705. doi:10.1366/000370207781393244

Arienzo, M. M., Swart, P. K., and Vonhof, H. B. (2013). Measurement of δ18O and δ2H values of fluid inclusion water in speleothems using cavity ring-down spectroscopy compared with isotope ratio mass spectrometry. *Rapid Commun. Mass Spectrom.* 27, 2616–2624. doi:10.1002/rcm.6723

Audétat, A., Günther, D., and Heinrich, C. A. (1998). Formation of a magmatic-hydrothermal ore deposit: insights with LA-ICP-MS analysis of fluid inclusions. *Science* 279, 2091–2094. doi:10.1126/science.279.5359.2091

Barker, C., and Torkelson, B. E. (1975). Gas adsorption on crushed quartz and basalt. *Geochimica Cosmochimica Acta* 39, 212–218. doi:10.1016/0016-7037(75)90173-8

Becker, J. A., Bickle, M. J., Galy, A., and Holland, T. J. B. (2008). Himalayan metamorphic CO2 fluxes: quantitative constraints from hydrothermal springs. *Earth Planet. Sci. Lett.* 265, 616–629. doi:10.1016/j.epsl.2007.10.046

Beeskow, B., Treloar, P., Rankin, A., Vennemann, T., and Spangenberg, J. (2006). A reassessment of models for hydrocarbon generation in the Khibiny nepheline syenite complex, Kola Peninsula, Russia. *Lithos* 91, 1–18. doi:10.1016/j.lithos.2006.03.006

Blamey, N. J. F. (2012). Composition and evolution of crustal, geothermal and hydrothermal fluids interpreted using quantitative fluid inclusion gas analysis. *J. Geochem. Explor.* 116–117, 17–27. doi:10.1016/j.gexplo.2012.03.001

Boutier, A., Martinez, I., Sissmann, O., Agostini, S., Daniel, I., Van Baalen, M., et al. (2024). Complexity of graphite formation in response to metamorphic methane generation and transformation in an orogenic ultramafic body. *Geochimica Cosmochimica Acta* 364, 166–183. doi:10.1016/j.gca.2023.10.028

Boutier, A., Vitale Brovarone, A., Martinez, I., Sissmann, O., and Mana, S. (2021). High-pressure serpentinization and abiotic methane formation in metaperidotite from the Appalachian subduction, northern Vermont. *Lithos* 396–397, 106190. doi:10.1016/j.lithos.2021.106190

Bräuer, K., Geissler, W. H., Kämpf, H., Niedermannn, S., and Rman, N. (2016). Helium and carbon isotope signatures of gas exhalations in the westernmost part of the Pannonian Basin (SE Austria/NE Slovenia): evidence for active lithospheric mantle degassing. *Chem. Geol.* 422, 60–70. doi:10.1016/j.chemgeo.2015.12.016

Calvin, K., Dasgupta, D., Krinner, G., Mukherji, A., Thorne, P. W., Trisos, C., et al. (2023). "IPCC, 2023: climate change 2023: synthesis report," in *Contribution of working groups I, II and III to the sixth assessment report of the intergovernmental panel on climate change core writing team. IPCC.* Editors H. Lee, and J. Romero (Geneva, Switzerland: Intergovernmental Panel on Climate Change). doi:10.59327/IPCC/AR6-9789291691647

Crossey, L., Karlstrom, K., Springer, A., Newell, D., Hilton, D., and Fischer, T. (2009). Degassing of mantle-derived CO2 and He from springs in the southern Colorado Plateau region-Neotectonic connections and implications for groundwater systems. *Geol. Soc. Am. Bull.* 121, 1034–1053. doi:10.1130/B26394.1

Cui, S., Wang, W., Cheng, C., Yao, Y., Qin, C., and Sun, Q. (2021). Raman quantitative measurement for carbon isotopic composition of CO2: theory and method. *Chem. Geol.* 585, 120570. doi:10.1016/j.chemgeo.2021.120570

de Graaf, S., Vonhof, H. B., Weissbach, T., Wassenburg, J. A., Levy, E. J., Kluge, T., et al. (2020). A comparison of isotope ratio mass spectrometry and cavity ring-down spectroscopy techniques for isotope analysis of fluid inclusion water. *Rapid Commun. Mass Spectrom.* 34, e8837. doi:10.1002/rcm.8837

Douglas, P. M. J., Stolper, D. A., Eiler, J. M., Sessions, A. L., Lawson, M., Shuai, Y., et al. (2017). Methane clumped isotopes: progress and potential for a new isotopic tracer. *Org. Geochem.* 113, 262–282. doi:10.1016/j.orggeochem.2017.07.016

Etiope, G., Ifandi, E., Nazzari, M., Procesi, M., Tsikouras, B., Ventura, G., et al. (2018). Widespread abiotic methane in chromitites. *Sci. Rep.* 8, 8728. doi:10.1038/s41598-018-27082-0

Ferrando, S., Frezzotti, M. L., Orione, P., Conte, R. C., and Compagnoni, R. (2010). Late-Alpine rodingitization in the Bellecombe meta-ophiolites (Aosta Valley, Italian Western Alps): evidence from mineral assemblages and serpentinization-derived H_2-bearing brine. *Int. Geol. Rev.* 52, 1220–1243. doi:10.1080/00206810903557761

Fiebig, J., Hofmann, S., Tassi, F., D'Alessandro, W., Vaselli, O., and Woodland, A. B. (2015). Isotopic patterns of hydrothermal hydrocarbons emitted from Mediterranean volcanoes. *Chem. Geol.* 396, 152–163. doi:10.1016/j.chemgeo.2014.12.030

Frezzotti, M. L., Tecce, F., and Casagli, A. (2012). Raman spectroscopy for fluid inclusion analysis. *J. Geochem. Explor.* 112, 1–20. doi:10.1016/j.gexplo.2011.09.009

Frezzotti, M.-L., and Touret, J. L. R. (2014). CO2, carbonate-rich melts, and brines in the mantle. *Geosci. Front.* 5, 697–710. doi:10.1016/j.gsf.2014.03.014

Fuex, A. N. (1980). Experimental evidence against an appreciable isotopic fractionation of methane during migration. *Phys. Chem. Earth* 12, 725–732. doi:10.1016/0079-1946(79)90153-8

Fullerton, K. M., Schrenk, M., Yücel, M., Manini, E., Fattorini, D., di Carlo, M., et al. (2019). *Plate tectonics drive deep biosphere microbial community composition.*

Goldstein, R. H. (2001). Fluid inclusions in sedimentary and diagenetic systems. *Lithos* 55, 159–193. doi:10.1016/S0024-4937(00)00044-X

Gonzalez, Y., Nelson, D. D., Shorter, J. H., McManus, J. B., Dyroff, C., Formolo, M., et al. (2019). Precise measurements of 12CH2D2 by tunable infrared laser direct absorption spectroscopy. *Anal. Chem.* 91, 14967–14974. doi:10.1021/acs.analchem.9b03412

Gottikh, R. P., Pisotskii, B. I., and Kulakova, I. I. (2006). Geochemistry of reduced fluids from alkaline igneous rocks of the Khibiny Pluton. *Dokl. Earth S. C.* 407, 298–303. doi:10.1134/S1028334X06020334

Graser, G., Potter, J., Köhler, J., and Markl, G. (2008). Isotope, major, minor and trace element geochemistry of late-magmatic fluids in the peralkaline Ilímaussaq intrusion, South Greenland. *Lithos* 106, 207–221. doi:10.1016/j.lithos.2008.07.007

Grozeva, N. G., Klein, F., Seewald, J. S., and Sylva, S. P. (2020). Chemical and isotopic analyses of hydrocarbon-bearing fluid inclusions in olivine-rich rocks. *Phil. Trans. R. Soc. A* 378, 20180431. doi:10.1098/rsta.2018.0431

Guilhaumou, N., Velde, B. D., and Bény, C. (1984). Raman microprobe analysis of gaseous inclusion in diagenetically recrystallized calcites. *Bull. Minéralogie* 107, 193–202. doi:10.3406/bulmi.1984.7751

Gunter, B. D., and Gleason, J. D. (1971). Isotope fractionation during gas chromatographic separations. *J. Chromatogr. Sci.* 9, 191–192. doi:10.1093/chromsci/9.3.191

Hansteen, T. H., and Schmincke, H.-U. (1998). *Multi-stage magma ascent beneath the Canary Islands: evidence from ¯uid inclusions*.

Hazen, R. M., and Schiffries, C. M. (2013). Why deep carbon? *Rev. Mineralogy Geochem.* 75, 1–6. doi:10.2138/rmg.2013.75.1

Higaki, S., Oya, Y., and Makide, Y. (2006). Emission of methane from stainless steel surface investigated by using tritium as a radioactive tracer. *Chem. Lett.* 35, 292–293. doi:10.1246/cl.2006.292

Horita, J. (2001). Carbon isotope exchange in the system CO2-CH4 at elevated temperatures. *Geochimica Cosmochimica Acta* 65, 1907–1919. doi:10.1016/S0016-7037(01)00570-1

Kalinkin, A. M., Politov, A. A., Boldyrev, V. V., Kalinkina, E. V., Makarov, V. N., and Kalinnikov, V. T. (2002). Mechanical activation of diopside in CO2. *Inorg. Mater.* 38, 163–167. doi:10.1023/A:1014021312359

Kelley, D. S., and Früh-Green, G. L. (2001). Volatile lines of descent in submarine plutonic environments: insights from stable isotope and fluid inclusion analyses. *Geochimica Cosmochimica Acta* 65, 3325–3346. doi:10.1016/S0016-7037(01)00667-6

Kerrick, D. M., and Caldeira, K. (1998). Metamorphic CO2 degassing from orogenic belts. *Chem. Geol.* 145, 213–232. doi:10.1016/S0009-2541(97)00144-7

Kettel, D. (1996). *A method for processing adsorbed methane stable isotope data from the near surface based on fractionation* ∗ , 319–336.

Kita, I. (1981). A new type ball mill made of pyrex glass. *Geochem. J.* 15, 289–291. doi:10.2343/geochemj.15.289

Klein, F., Grozeva, N. G., and Seewald, J. S. (2019). Abiotic methane synthesis and serpentinization in olivine-hosted fluid inclusions. *Proc. Natl. Acad. Sci. U.S.A.* 116, 17666–17672. doi:10.1073/pnas.1907871116

Kogler, M., Köck, E.-M., Perfler, L., Bielz, T., Stöger-Pollach, M., Hetaba, W., et al. (2014). Methane decomposition and carbon growth on Y_2O_3, yttria-stabilized zirconia, and ZrO_2. *Chem. Mat.* 26, 1690–1701. doi:10.1021/cm404062r

Kueter, N., Schmidt, M. W., Lilley, M. D., and Bernasconi, S. M. (2019). Experimental determination of equilibrium CH4–CO2–CO carbon isotope fractionation factors (300–1200 °C). *Earth Planet. Sci. Lett.* 506, 64–75. doi:10.1016/j.epsl.2018.10.021

Kueter, N., Schmidt, M. W., Lilley, M. D., and Bernasconi, S. M. (2020). Kinetic carbon isotope fractionation links graphite and diamond precipitation to reduced fluid sources. *Earth Planet. Sci. Lett.* 529, 115848. doi:10.1016/j.epsl.2019.115848

Lamb, W. M., Valley, J. W., and Brown, P. E. (1987). Post-metamorphic CO2-rich fluid inclusions in granulites. *Contr. Mineral. Petrol.* 96, 485–495. doi:10.1007/BF01166693

Lambrecht, G., Diamond, L. W., and Pettke, T. (2008). Modification of gas speciation in quartz-hosted fluid inclusions by stray laser radiation during LA-ICPMS analysis. *Am. Mineralogist* 93, 1187–1190. doi:10.2138/am.2008.2960

Lee, H., Kim, H., Kagoshima, T., Park, J.-O., Takahata, N., and Sano, Y. (2019). Mantle degassing along strike-slip faults in the Southeastern Korean Peninsula. *Sci. Rep.* 9, 15334. doi:10.1038/s41598-019-51719-3

Li, L., Vozniuk, O., Cao, Z., Losch, P., Felderhoff, M., and Schüth, F. (2023). Hydrogenation of different carbon substrates into light hydrocarbons by ball milling. *Nat. Commun.* 14, 5257. doi:10.1038/s41467-023-40915-5

Li, W., Lu, S., Li, J., Feng, W., Zhang, P., Wang, J., et al. (2022a). Concentration loss and diffusive fractionation of methane during storage: implications for gas sampling and isotopic analysis. *J. Nat. Gas Sci. Eng.* 101, 104562. doi:10.1016/j.jngse.2022.104562

Li, W., Lu, S., Li, J., Wei, Y., Zhao, S., Zhang, P., et al. (2022b). Research progress on isotopic fractionation in the process of shale gas/coalbed methane migration. *Petroleum Explor. Dev.* 49, 1069–1084. doi:10.1016/S1876-3804(22)60333-1

Liati, A., Gebauer, D., and Fanning, C. (2000). U-Pb SHRIMP dating of zircon from the Novate granite (Bergell, Central Alps): evidence for Oligocene-Miocene magmatism, Jurassic/Cretaceous continental rifting and opening of the Valais trough. *Schweiz. Mineral. Petrogr. Mitte* 80, 305–316.

Liu, P., Wang, X., Lin, Y., Liu, C., Li, X., and Liu, W. (2020). Chemical and carbon isotope fractionations of alkane gases desorbed from confined systems and the application toward shale gas reservoir. *Mar. Petroleum Geol.* 113, 104103. doi:10.1016/j.marpetgeo.2019.104103

Luciani, N., van der Lubbe, J. H. L., Verdegaal-Warmerdam, S. J. A., Postma, O., Nikogosian, I. K., Davies, G. R., et al. (2022). Carbon and oxygen isotope analysis of CO2 trapped in silicate minerals. *Chem. Geol.* 602, 120872. doi:10.1016/j.chemgeo.2022.120872

Lüders, V., Plessen, B., and di Primio, R. (2012). Stable carbon isotopic ratios of CH4–CO2-bearing fluid inclusions in fracture-fill mineralization from the Lower Saxony Basin (Germany) – a tool for tracing gas sources and maturity. *Mar. Petroleum Geol.* 30, 174–183. doi:10.1016/j.marpetgeo.2011.10.006

Mangenot, X., Tarantola, A., Mullis, J., Girard, J.-P., Le, V.-H., and Eiler, J. M. (2021). Geochemistry of clumped isotopologues of CH4 within fluid inclusions in Alpine tectonic quartz fissures. *Earth Planet. Sci. Lett.* 561, 116792. doi:10.1016/j.epsl.2021.116792

Mironova, O. F. (2010). Volatile components of natural fluids: evidence from inclusions in minerals: methods and results. *Geochem. Int.* 48, 83–90. doi:10.1134/S0016702910010052

Mullis, J., Dubessy, J., Poty, B., and O'Neil, J. (1994). Fluid regimes during late stages of a continental collision: physical, chemical, and stable isotope measurements of fluid inclusions in fissure quartz from a geotraverse through the Central Alps, Switzerland. *Geochimica Cosmochimica Acta* 58, 2239–2267. doi:10.1016/0016-7037(94)90008-6

Nadeau, S., Philippot, P., and Pineau, F. (1993). Fluid inclusion and mineral isotopic compositions (HCO) in eclogitic rocks as tracers of local fluid migration during high-pressure metamorphism. *Earth Planet. Sci. Lett.* 114, 431–448. doi:10.1016/0012-821X(93)90074-J

Nivin, V. A. (2019). Occurrence forms, composition, distribution, origin and potential hazard of natural hydrogen–hydrocarbon gases in ore deposits of the khibiny and lovozero massifs: a review. *Minerals* 9, 535. doi:10.3390/min9090535

Norman, D. I., and Sawkins, F. J. (1987). Analysis of volatiles in fluid inclusions by mass spectrometry. *Chem. Geol.* 61, 1–10. doi:10.1016/0009-2541(87)90020-9

Normand, C., and Williams-Jones, A. E. (2007). Physicochemical conditions and timing of rodingite formation: evidence from rodingite-hosted fluid inclusions in the JM Asbestos mine, Asbestos, Québec. *Geochem Trans.* 8, 11. doi:10.1186/1467-4866-8-11

Ono, S., Wang, D. T., Gruen, D. S., Lollar, B. S., Zahniser, M. S., McManus, B. J., et al. (2014). Measurement of a doubly substituted methane isotopologue, 13CH3D, by tunable infrared laser direct absorption spectroscopy. *Anal. Chem.* 86 (13), 6487–6494. doi:10.1021/ac5010579

Peretti, A., Dubessy, J., Mullis, J., Frost, B. R., and Trommsdorff, V. (1992). Highly reducing conditions during Alpine metamorphism of the Malenco peridotite (Sondrio, northern Italy) indicated by mineral paragenesis and H2 in fluid inclusions. *Contr. Mineral. Petrol.* 112, 329–340. doi:10.1007/BF00310464

Petersilie, I. A., and Sörensen, H. (1970). Hydrocarbon gases and bituminous substances in rocks from the Ilímaussaq alkaline intrusion, South Greenland. *Lithos* 3, 59–76. doi:10.1016/0024-4937(70)90088-5

Piperov, N. B., and Penchev, N. P. (1973). A study on gas inclusions in minerals. Analysis of the gases from micro-inclusions in allanite. *Geochimica Cosmochimica Acta* 37, 2075–2097. doi:10.1016/0016-7037(73)90009-4

Potter, J., and Longstaffe, F. J. (2007). A gas-chromatograph, continuous flow-isotope ratio mass-spectrometry method for δ13C and δD measurement of complex fluid inclusion volatiles: examples from the Khibina alkaline igneous complex, northwest Russia and the south Wales coalfields. *Chem. Geol.* 244, 186–201. doi:10.1016/j.chemgeo.2007.06.014

Potter, J., Rankin, A. H., and Treloar, P. J. (2004). Abiogenic Fischer–Tropsch synthesis of hydrocarbons in alkaline igneous rocks; fluid inclusion, textural and isotopic evidence from the Lovozero complex, N.W. Russia. *Lithos* 75, 311–330. doi:10.1016/j.lithos.2004.03.003

Rella, C. W., Hoffnagle, J., He, Y., and Tajima, S. (2015). Local- and regional-scale measurements of CH_4, $\delta^{13}CH_4$, and C_2H_6 in the Uintah Basin using a mobile stable isotope analyzer. *Atmos. Meas. Tech.* 8, 4539–4559. doi:10.5194/amt-8-4539-2015

Remigi, S., Frezzotti, M.-L., Rizzo, A. L., Esposito, R., Bodnar, R. J., Sandoval-Velasquez, A., et al. (2023). Spatially resolved CO2 carbon stable isotope analyses at the microscale using Raman spectroscopy. *Sci. Rep.* 13, 18561. doi:10.1038/s41598-023-44903-z

Rigopoulos, I., Ioannou, I., Delimitis, A., Efstathiou, A., and Kyratsi, T. (2018). Ball milling effect on the CO2 uptake of mafic and ultramafic rocks: a review. *Geosciences* 8, 406. doi:10.3390/geosciences8110406

Roedder, E. (1984). *Fluid inclusions: an introduction to studies of all types of fluid inclusions, gas, liquid, or melt, trapped in materials from earth and space, and their application to the understanding of geologic processes, Reviews in mineralogy*. Blacksburg, Va: Mineralogical Soc. of America.

Rosenkranz, S., Breitung-Faes, S., and Kwade, A. (2011). Experimental investigations and modelling of the ball motion in planetary ball mills. *Powder Technol.* 212, 224–230. doi:10.1016/j.powtec.2011.05.021

Sackett, W. M., and Chung, H. M. (1979). Experimental confirmation of the lack of carbon isotope exchange between methane and carbon oxides at high temperatures. *Geochimica Cosmochimica Acta* 43, 273–276. doi:10.1016/0016-7037(79)90246-1

Sackett, W. M., and Conkright, M. E. (1997). Summary and re-evaluation of the high-temperature isotope geochemistry of methane. *Geochimica Cosmochimica Acta* 61, 1941–1952. doi:10.1016/S0016-7037(97)00039-2

Salvi, S., and Williams-Jones, A. (2003). "Bulk analysis of volatiles in fluid inclusions," in *Fluid inclusions: analysis and interpretation* (Quebec: Mineralogical Association of Canada), 10–11.

Sanz-Robinson, J., Brisco, T., Warr, O., Jabeen, I., Lacrampe-Couloume, G., Hanley, J. J., et al. (2021). Advances in carbon isotope analysis of trapped methane and volatile hydrocarbons in crystalline rock cores. *Rapid Comm. Mass Spectrom.* 35, e9170. doi:10.1002/rcm.9170

Sawama, Y., Niikawa, M., Ban, K., Park, K., Aibara, S., Itoh, M., et al. (2020). Quantitative mechanochemical methanation of CO_2 with H_2O in a stainless steel ball mill. *BCSJ* 93, 1074–1078. doi:10.1246/bcsj.20200105

Scambelluri, M., and Philippot, P. (2001). Deep fluids in subduction zones. *Lithos* 55, 213–227. doi:10.1016/S0024-4937(00)00046-3

Schmidt, R., Martin Scholze, H., and Stolle, A. (2016). Temperature progression in a mixer ball mill. *Int. J. Ind. Chem.* 7, 181–186. doi:10.1007/s40090-016-0078-8

Shi, G. U., Tropper, P., Cui, W., Tan, J., and Wang, C. (2005). Methane (CH4)-bearing fluid inclusions in the Myanmar jadeitite. *Geochem. J.* 39, 503–516. doi:10.2343/geochemj.39.503

Sobolev, N. V., Logvinova, A. M., Tomilenko, A. A., Wirth, R., Bul'bak, T. A., Luk'yanova, L. I., et al. (2019). Mineral and fluid inclusions in diamonds from the Urals placers, Russia: evidence for solid molecular N2 and hydrocarbons in fluid inclusions. *Geochimica Cosmochimica Acta* 266, 197–219. doi:10.1016/j.gca.2019.08.028

Stolper, D. A., Lawson, M., Formolo, M. J., Davis, C. L., Douglas, P. M. J., and Eiler, J. M. (2018). The utility of methane clumped isotopes to constrain the origins of methane in natural gas accumulations. *Geol. Soc.* 468, 23–52. doi:10.1144/SP468.3

Stuart, F. M., and Turner, G. (1992). The abundance and isotopic composition of the noble gases in ancient fluids. *Chem. Geol. Isot. Geosci. Sect.* 101, 97–109. doi:10.1016/0009-2541(92)90207-L

Tarantola, A., Mullis, J., Vennemann, T., Dubessy, J., and de Capitani, C. (2007). Oxidation of methane at the CH4/H2O–(CO2) transition zone in the external part of the Central Alps, Switzerland: evidence from stable isotope investigations. *Chem. Geol. New Results Fluid Melt Inclusion Res.* 237, 329–357. doi:10.1016/j.chemgeo.2006.07.007

Touret, J., and Dietvorst, P. (1983). Fluid inclusions in high-grade anatectic metamorphites. *JGS* 140, 635–649. doi:10.1144/gsjgs.140.4.0635

Touret, J. L. R., and Frezzotti, M.-L. (2003). "Fluid inclusions in high pressure and ultrahigh pressure metamorphic rocks," in *Ultrahigh pressure metamorphism. Mineralogical society of great britain and Ireland*. Editors G. Papp, T. G. Weiszburg, D. A. Carswell, R. Compagnoni, and F. Rolfo (Budapest: Mineralogical Society of Great Britain and Ireland), 467–487. doi:10.1180/EMU-notes.5.15

van den Kerkhof, A., Kronz, A., and Simon, K. (2014). Deciphering fluid inclusions in high-grade rocks. *Geosci. Front.* 5, 683–695. doi:10.1016/j.gsf.2014.03.005

Veen, A. M. H., Zalewska, E. T., Osselen, D. R. V., Fernández, T. E., Gómez, C., Beránek, J., et al. (2020). International comparison CCQM-K112 biogas. *Metrologia* 57, 08011. doi:10.1088/0026-1394/57/1A/08011

Villa, I. M. (2001). Radiogenic isotopes in fluid inclusions. *Lithos* 55, 115–124. doi:10.1016/S0024-4937(00)00041-4

Vitale Brovarone, A., Martinez, I., Elmaleh, A., Compagnoni, R., Chaduteau, C., Ferraris, C., et al. (2017). Massive production of abiotic methane during subduction evidenced in metamorphosed ophicarbonates from the Italian Alps. *Nat. Commun.* 8, 14134. doi:10.1038/ncomms14134

Vitale Brovarone, A., Sverjensky, D. A., Piccoli, F., Ressico, F., Giovannelli, D., and Daniel, I. (2020). Subduction hides high-pressure sources of energy that may feed the deep subsurface biosphere. *Nat. Commun.* 11, 3880. doi:10.1038/s41467-020-17342-x

Volk, H., Fuentes, D., Fuerbach, A., Miese, C., Koehler, W., Bärsch, N., et al. (2010). First on-line analysis of petroleum from single inclusion using ultrafast laser ablation. *Org. Geochem.* 41, 74–77. doi:10.1016/j.orggeochem.2009.05.006

Wang, W., and Lu, W. (2023). High-precision analysis of carbon isotopic composition for individual CO2 inclusions via Raman spectroscopy to reveal the multiple-stages evolution of CO2- bearing fluids and melts. *Geosci. Front.* 14, 101528. doi:10.1016/j.gsf.2022.101528

Wang, X., Hu, W., Qiu, Y., Liu, Y., Jia, D., Cao, J., et al. (2022). Fluid inclusion evidence for extreme overpressure induced by gas generation in sedimentary basins. *Geology* 50, 765–770. doi:10.1130/G49848.1

Weissbach, T., Kluge, T., Affolter, S., Leuenberger, M. C., Vonhof, H., Riechelmann, D. F. C., et al. (2023). Constraints for precise and accurate fluid inclusion stable isotope analysis using water-vapour saturated CRDS techniques. *Chem. Geol.* 617, 121268. doi:10.1016/j.chemgeo.2022.121268

Welhan, J. A. (1988). Methane and hydrogen in mid-ocean-ridge basalt glasses: analysis by vacuum crushing. *Can. J. Earth Sci.* 25, 38–48. doi:10.1139/e88-004

Young, E. D., Kohl, I. E., Lollar, B. S., Etiope, G., Rumble, D., Li, S., Haghnegahdar, M. A., Schauble, E. A., McCain, K. A., Foustoukos, D. I., Sutclife, C., Warr, O., Ballentine, C. J., Onstott, T. C., Hosgormez, H., Neubeck, A., Marques, J. M., Pérez-Rodríguez, I., Rowe, A. R., LaRowe, D. E., Magnabosco, C., Yeung, L. Y., Ash, J. L., and Bryndzia, L. T. (2017). The relative abundances of resolved l2CH2D2 and 13CH3D and mechanisms controlling isotopic bond ordering in abiotic and biotic methane gases. *Geochimica Cosmochimica Acta* 203, 235–264. doi:10.1016/j.gca.2016.12.041

Zhang, L., Wang, Q., Ding, X., and Li, W.-C. (2021). Diverse serpentinization and associated abiotic methanogenesis within multiple types of olivine-hosted fluid inclusions in orogenic peridotite from northern Tibet. *Geochimica Cosmochimica Acta* 296, 1–17. doi:10.1016/j.gca.2020.12.016

Zhang, L., Wang, Q., Mikhailenko, D. S., Ding, X., Li, W.-C., and Xian, H. (2022). Hydroxychloride-bearing fluid inclusions in ultramafic rocks from New Caledonia: implications for serpentinization in saline environments on Earth and beyond. *J. Geophys. Res. Solid Earth* 127, e2022JB024508. doi:10.1029/2022JB024508

Zhang, T., and Krooss, B. M. (2001). Experimental investigation on the carbon isotope fractionation of methane during gas migration by diffusion through sedimentary rocks at elevated temperature and pressure. *Geochimica Cosmochimica Acta* 65, 2723–2742. doi:10.1016/S0016-7037(01)00601-9

Zhang, T., Yang, R., Milliken, K. L., Ruppel, S. C., Pottorf, R. J., and Sun, X. (2014). Chemical and isotopic composition of gases released by crush methods from organic rich mudrocks. *Org. Geochem.* 73, 16–28. doi:10.1016/j.orggeochem.2014.05.003

Zolensky, M. E., Bodnar, R. J., Yurimoto, H., Itoh, S., Fries, M., Steele, A., et al. (2017). The search for and analysis of direct samples of early Solar System aqueous fluids. *Philosophical Trans. R. Soc. A Math. Phys. Eng. Sci.* 375, 20150386. doi:10.1098/rsta.2015.0386